EFFECT OF ANNEALING TEMPERATURE ON THE PERFORMANCE OF ZnO BASED DYE SENSITIZE SOLAR CELL

by

MD. SHAHADATH HOSSAIN

NAZIM UDDIN

BACHELOR OF SCIENCE IN ELECTRICAL AND ELECTRONIC ENGINEERING

Department of Electrical and Electronic Engineering
INTERNATIONAL ISLAMIC UNIVERSITY CHITTAGONG

JULY 2022

EFFECT OF ANNEALING TEMPERATURE ON THE PERFORMANCE OF ZnO BASED DYE SENSITIZE SOLAR CELL

by

MD. SHAHADATH HOSSAIN

NAZIM UDDIN

A thesis
submitted as partial fulfilment of the requirement for the degree of

BACHELOR OF SCIENCE IN ELECTRICAL AND ELECTRONIC ENGINEERING

Department of Electrical and Electronic Engineering
INTERNATIONAL ISLAMIC UNIVERSITY CHITTAGONG

JULY 2022

CERTIFICATE OF APPROVAL

The thesis/project entitled as "**Effect of annealing temperature on the performance of ZnO based Dye sensitize solar cell**" submitted by **Md. Shahadath Hossain**, bearing Matric ID. **ET173008** and **Nazim Uddin**, bearing Matric **ID. ET173013** of session **Spring 2021**, to the Department of Electrical and Electronic Engineering, International Islamic University Chittagong, has been accepted as satisfactory in partial fulfilment of the requirements for the degree of Bachelor of Science in Engineering and approved for the examination held on **22nd July, 2022**.

_____

Supervisor
Dr. Md. Shamimul Haque Choudhury
Associate Professor,
Department of Electrical and Electronic Engineering
International Islamic University Chittagong.

DECLARATION

It is officially stated that all of the work included in this thesis/project has been completed by us and has not been submitted to any other institution for the granting of any degree or certificate.

_____

Md. Shahadath Hossain

_____

Nazim Uddin

ACKNOWLEDGMENT

To begin, we would like to offer our appreciation to Allah (SWT), the Almighty, Merciful, and Benevolent, for His benefaction and blessing on us, which allowed us to conduct this study. We received kind and spontaneous supervision, advice, and support from the following individuals while performing our research and writing our dissertation, and we would like to use this opportunity to express our thanks to them. Our supervisor, Dr. Md. Shamimul Haque Choudhury, was instrumental in helping us complete our thesis. Not only has he supported, inspired, and motivated us for the whole of the class, but he also has confidence in our capacity to successfully complete a research paper on the subject of this thesis. He has contributed essential insights and commentary on the thesis. We would want to offer our heartfelt appreciation to him for his advise, assistance, patience, and understanding during the whole study process. We owe him a particular gratitude in this respect since he gave us the opportunity to hone our research and statistical software skills. In addition, we would like to express our appreciation to the EEE department faculty for all of the help that they provided in this regard. Everyone who helped us develop our study and write this dissertation is to be thanked for their contributions. We would like to thank all of our family members, especially our parents, sisters, and brothers, for their assistance with our study. We are grateful to them all for making it possible for us to conduct this study and have such an enriching experience.

Authors

ABSTRACT

Within this study, we explore the effects of annealing temperature on the overall performance of ZnO-based dye-sensitized solar cells. The Electrophoretic Deposition Method (EPD) was used to prepare the photo-electrodes. As a post-deposition treatment, the electrodeposited photo anodes were annealed at various annealing temperatures ranging from 100 to 500 ℃. When annealing temperature is increased, the open circuit voltage, short circuit current density increase. As a result, the fill factor and the overall efficiency also improved (from 1.59 to 2.21%). The series resistance of the cells (calculated from Dark data) reduces by increasing the annealing temperature up to 400 ℃. Similar results have been observed from the calculated series resistance from the I-V curve, which is the reason for the change in the photovoltaic performance. On the other hand, the shunt resistance of the cell (calculated from Dark data) increases by increasing the annealing temperature up to 400 ℃. The same results have been observed from the calculated shunt resistance from the I-V curve, which is the reason for the change in the photovoltaic performance. We also determine ideality factor and barrier height using different methods such as the Cheung_Cheung function and Norde method. The ideality factor affects the fill factor of the solar cell; when n increases, the fill factor decreases and eventually affects the efficiency. Also, there is a linear relationship between the ideality factor and barrier height. The increasing temperature up to 400 ℃ gives a lower ideality factor and higher barrier height. Moreover, the series and shunt resistance under illumination shows different values from the dark condition but follows the same trend. Under both dark and illumination conditions, the photovoltaic performance data is identical to the series and shunt resistance data.

TABLE OF CONTENTS

TABLES

LIST OF FIGURES

LIST OF ABBREVIATIONS

DSSC	Dye Sensitized Solar Cell
ZnO	Zinc Oxide
TCO	Transparent Conductive Oxide
FTO	Fluorine-doped Tin Oxide
SEM	Scanning Electron Microscope
MPa	Mega pascal
AM	Air Mass
EPD	Electrophoretic Deposition
SBH	Schottky Barrier Height
NP	Nanoparticle
PCE	Power Conversion Efficiency

CHAPTER 1

INTRODUCTION

1.1 Introduction

The sun's nuclear fusion generates solar energy. For human consumption, such as producing energy, it is essential to the survival of all species on Earth. The increasing energy demand of our civilization could be adequately met by the development of solar cells that harness solar energy. Recently, people have started to pay more attention to solar photovoltaic technology as a possible alternative energy source for the future. Since O'Regan and Gratzel published the initial study on dye-sensitized solar cells (DSSCs) in 1991, more than two decades have passed [1]. Dye-sensitized solar cells (DSSCs) are key power devices designed to address numerous environmental and energy concerns. A dye-sensitized solar cell, also known as a DSSC, is composed of three thin layers that are next to one another. An organic liquid electrolyte is made up of three layers: a photosensitive TiO_2 film, an adsorbable dye, and an organic liquid electrolyte containing iodides and triiodides as the redox pair [2]. ZnO-based DSSCs are being studied as third-generation solar cells due to their commercial viability, low cost, and simple manufacturing. It has a lower recombination probability and higher electron mobility than TiO_2, which is its main competitor. Solar cells made from ZnO can be made for a low-price using materials that are good for the environment, like ZnO and natural dyes made from nearby fruits and flowers. Despite the fact that ZnO-based DSSCs containing natural dyes are less efficient, intensive research has been performed to reduce the cost of DSSCs while maintaining the same efficiency as silicon-based solar cells. The total performance of DSSCs is determined by various parameters, including dye adsorption in ZnO nanostructures and dye absorption spectrum [3]. Low-cost thin-film solar cells, such as dye-sensitized cells, are available. A photo - electrochemical system uses a semiconductor that is produced between an anode and an electrolyte that has been photo-sensitized to work. The The DSSC has a lot of good qualities, like how easy it is to make with traditional roll printing, how it is semi-flexible and semi-transparent, so it can be used in ways that glass-based systems can't, and how most of the materials used are cheap [4]. There have been three components to the DSSC: the photoelectrode, which is made of a transparent conducting oxide (TCO), the organic dye molecules that are used to collect light and the electrolyte that is used to excite the charges in the electrolyte on the

electrode surface. A significant portion of how well DSSC functions is determined by the characteristics of the interfaces that exist between its many components. Another primary advantage of utilizing a nanostructured material is that it provides dyes with a large amount of available area to adhere to, allowing them to take in the most amount of light possible. As an exciting alternative wide band gap material, Zinc Oxide (ZnO) may be manufactured in a variety of nanostructures and has a band gap that is similar to that of TiO_2. This allows for greater versatility in the construction of various DSSC solar cells for the purpose of enhancing the efficiency and durability of these cells [5]. Solar cells that employ dyes to absorb light have been developed and improved over the past decade by researchers. DSSC technology has been used to convert solar energy into electricity. The efficiency of electricity conversion for the traditional silicon solar cells ranged anywhere from 10 to 34 percent. Despite the fact that silicon-based solar cells have good photovoltaic performance, their usefulness is limited due to the high prices of sophisticated fabrication designs. With their excellent optical and photovoltaic properties, DSSCs made of polymers have been proposed as an inexpensive alternative to silicon solar cells. They have a high efficiency of converting photon power to electric power (11–12 percent in the lab), good stability, and long-term reliability [6]. These photovoltaic devices are suited for mass manufacturing due to their ease of fabrication and possibly low production costs. In the most common DSSC, an iodide-triiodide (I^-/I_3^-) liquid electrolyte separates a nanoparticle TiO_2 photoelectrode and a platinum counter electrode. Zinc oxide has recently become a possible alternative to TiO_2 as a material for semiconductors. This is because ZnO-based DSSCs have improved in performance in recent years. When compared to anatase TiO_2, the charge transport speed of ZnO is much faster, and its electron mobility is orders of magnitude higher than that of anatase TiO_2. These are two of the potential advantages that could be gained from employing ZnO in DSSCs. This property should allow for high charge collection efficiency and make altering the redox shuttle easier in future solar cells with higher (Voc) [7].

ZnO-based DSSCs' power conversion efficiency can be improved by increasing the annealing temperature of the photoelectrode layer. ZnO nanoparticle crystallinity can be improved by annealing treatment without affecting their phase and eliminating impurity [8]. For each DSSC, there is a resistor in series (Rs) and a separate resistor in series (Rsh). This means that the most efficient DSSCs should have a high Rsh and low Rs. Fill factor (FF) can be increased by raising Rsh value, whereas increasing Rs value can lower it. A

DSSC's Rsh value tells us how the IDC is caused by the reverse electron transfer, and as the IDC decreases, the Rsh value increases. The Jsc value falls when the Rs value of the DSSC grows, or the Rs value of the DSSC declines. The DSSC's energy conversion efficiency (percentage) drops due to the declining Jsc. In the case of an ideal solar cell, the FF value is 1and efficiency is 100%. Also, its Rsh value is infinite [9]. DSSCs with ZnO photo-electrodes made using ethanol-based paste had a highest efficiency of 0.11 percent (Voc = 232.4 mV, Jsc = 111.6 A/cm^2, FF = 61.41 percent) [10].

When it comes to DSSCs, we want to know how the temperature of the ZnO nanoparticle-based photoelectrode affects its performance in both the dark and the light. Electrophoretic deposition (EPD) analysis is used to determine the effect of annealing temperatures on the charge transport properties of ZnO-based DSSCs. The *J-V* curves of DSSCs were analyzed and described how they altered in relation to each other. The photovoltaic performances of the DSSCs were used to investigate the links between the IDC, Rs, and Rsh and the FF. The development of materials that would improve the DSSC's conversion efficiency, simplify production, and ensure their long life is also a major focus of this study."

1.2 Objectives

- To understand the construction and working principle of Dye Sensitized Solar Cell.
- To understand the detail study of different analysis method.
- To determine different parameters from dark *I-V* curve of ZnO-based DSSC.
- To understand the comparison between different parameters of dark *I-V* curve by different methods.

1.3 Outline of the work

Fig. 1.1 show the outline diagram of this work

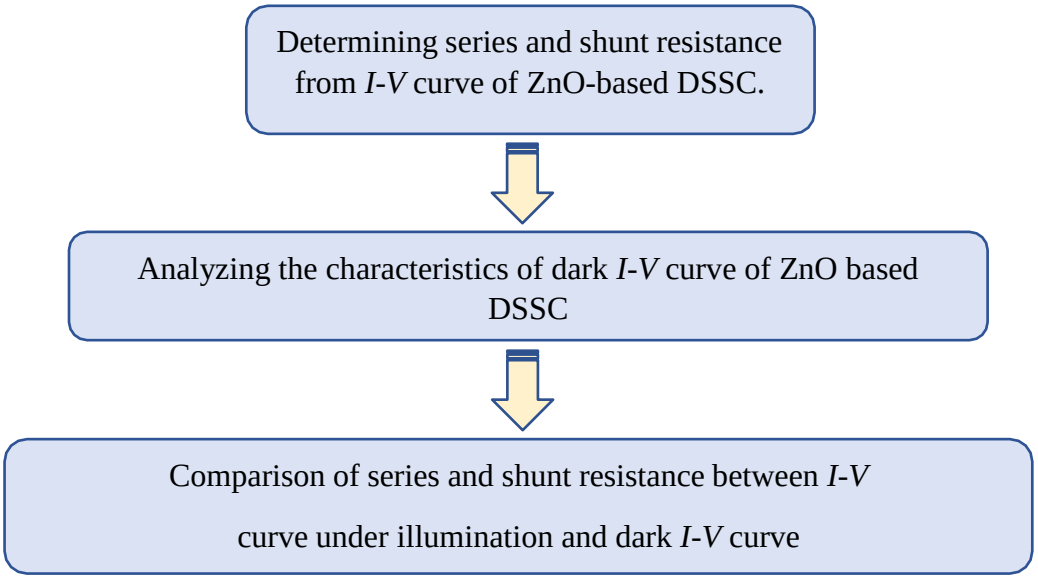

Fig. 1.1: Outline of the work

1.4 Thesis Layout

Research on ZnO-based solar cells and the influence of No annealing temperature on their performance has been divided into the following six chapters. Here is a quick synopsis of each chapter:

Chapter one provides a summary of the entire work, including the introduction, objectives, work diagram, and thesis layout.

Chapter two discuss about literature review, introduction of ZnO, the underlying theories and fundamental properties of ZnO. It also explains different application of ZnO and its future.

Chapter three gives a brief description of the parameters of dark current-voltage analysis.

Chapter four provides the investigation of the experimental work that has been done.

Chapter five contains results and discussion on dark Current-Voltage analysis of ZnO-based DSSC under dark condition and illumination.

Chapter six provides the summary according to the finding of this study.

CHAPTER 2

LITERATURE REVIEW

2.1 Introduction

Renewable sources of heat and electricity can be generated without releasing greenhouse emissions by converting sunlight into heat and electricity [11], [12]. The latest generation of solar cells known as Dye-Sensitized Solar Cells (DSSCs) is seen as an economically viable replacement to the old solar cell architecture. Because of the many advantages it offers, scholars have contributed a great time and energy to developing DSSCs that are more effective [13], [14]. Michael Gratzel and Brian O'Regan invented this cell, which is also known as the Gratzel cell. It is part of the family of solar cells made from thin films. This new DSSC alternative energy source is predicted to have a substantial impact on overall energy production in the future years. One of the primary reasons for this is the availability of low-cost fabrication and other appealing characteristics, such as transparency and adaptability, that may make it easier to break into the market. Even though DSSCs are projected to have a 20% power conversion efficiency (PCE), there remains scope for improvements [15]. More than three decades of research on DSSCs have focused on increasing their efficiency and making them more suitable for real-world applications. The photoanode, counter electrode, electrolyte, and photosensitizer (dye) are all included in a DSSC [16], [17]. One technology that has proved to reach moderate efficiency among all of them is DSSCs; as such, they can compete with conventional cells. DSSC uses a light-absorbing sensitizer in collaboration with a wide band-gap semiconductor to combine optical absorption with charge separation.

2.2 Solar cell

Any device that directly converts the energy of light into electrical energy through the photovoltaic effect can be referred to as a solar cell. Solar cells are also known as photovoltaic cells. The earth gets an enormous amount of solar power. An ordinary star, the sun has been burning for 4 billion years as a fusion reactor. It is considered to be a typical star. It generates an amount of power in one minute that is sufficient to meet the annual energy requirements of the entire world. It delivers more energy in a single day than our existing population would use in the next 27 years if it continued to exist. In

point of fact, "the quantity of solar radiation reaching the globe over the course of three days is equivalent to the energy stored in all fossil fuel sources." The concept of capturing the limitless and costless power of the sun is still a comparatively new concept. Solar power generators are simply given to residences, educational institutions, and commercial establishments, where their installation does not call for any additional construction or land area and where their operation is safe and unobtrusive. More solar energy capacity can be added to communities as they continue to grow. Today, developing nations are the most interested in solar energy, making up the market sector for photovoltaics that is expanding at the quickest rate. Solar power is the logical alternative for energy, as people live without electricity when the sun beats down on the land. "Governments are finding its modular, decentralized character suitable for satisfying the electric needs." People in rural places who cannot afford conventional energy can use solar power instead of extending expensive power lines. With solar electricity, there are just two important issues to consider: the amount of sunshine available and the associated equipment costs. Location, season, time of day, and cloud cover all affect the quantity of sunlight a place receives. In light of the significance of utilizing solar cells and making effective use of solar energy, we will take a look at the many kinds of solar cells that are now available in this article. A solar cell, also known as a photovoltaic cell, is an electronic device that directly converts the energy of light into electricity by using the photovoltaic effect, which is both a physical and chemical process. It is a type of photoelectric cell, which is a device whose electrical characteristics, such as current, voltage, or resistance, change when exposed to light. Photoelectric cells are described as devices whose electrical characteristics change when exposed to light. Photovoltaic modules, often known as solar panels, are assembled from solar cells. Solar cells are the fundamental element of this technology. Whether the light comes from the sun or from an artificial source, solar cells are still considered to be photovoltaic. They can detect light or other forms of electromagnetic radiation that are located close to the visible spectrum, and they can also measure the amount of light that is present. One example of their use is in infrared detectors. In order for a photovoltaic (PV) cell to function properly, there are three fundamental characteristics that must be present:

1) The process of absorbing light, which results in the generation of electron-hole pairs or exactions.

2) The splitting of charge carriers into their respective categories
3) The individual extraction of those carriers into a circuit that is external [18].

There must be a certain amount of energy that can be captured by solar cells in order to be effective. A wide range in the visible region of the solar spectrum (400-700nm) is present for air masses (AM) 0, which means that solar cells should aim to absorb as much of this light as possible. The solar spectrum ranges from 100 nanometers to one millimeter, but most of the irradiance occurs between 250 and 2500 nanometers (**Fig. 2.1**).

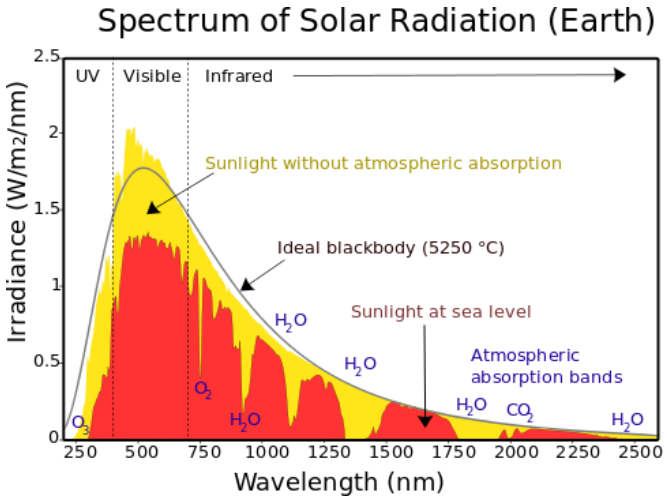

Fig. 2.1 Solar irradiance spectrum above atmosphere and at surface

2.2.1 Construction of Solar Cell

Although this is essentially a junction diode, it is constructed differently from a normal p-n junction diode. P-type semiconductors are formed on top of n-type semiconductors that are much thicker than the first layer. On top of the p-type semiconductor layer, a few finer electrodes placed for better performance. The thin p-type layer is not impeded by these electrodes. A p-n junction is located just below the p-type layer. At the bottom of the n-type layer, an electrode is placed for collecting current. To guard against mechanical damage to the solar cell, the entire assembly enclose with a thin sheet of glass.

2.2.2 Working principle of solar cell

It is possible for photons of light to quickly access the P-N junction through the very thin p-type layer when they reach it. An electron-hole pair can be formed with enough

energy from photons that are released by the light energy. The thermal balance of the connection is disrupted by the incident light. The depletion region's free electrons can swiftly go to the n-type side of the junction by crossing the junction. It is possible for the depletion holes to reach the p-type side of the junction in an extremely short period of time. Once they reach the n-type side, the freshly formed free electrons are unable to cross the junction due to the junction's barrier potential. When new holes are made on the p-type side, they will not be able to cross the junction because of the same barrier potential as the original. In other words, the n-type side of the junction has a larger density of electrons, while the p-type side has a higher density of holes, and as a result, the p-n junction acts like a tiny battery cell. Photovoltage is the term for the voltage that's been set up. Connecting a small load to the junction will result in very little current flowing [20]. **Fig. 2.2** show the schematic diagram of the solar cell working principle.

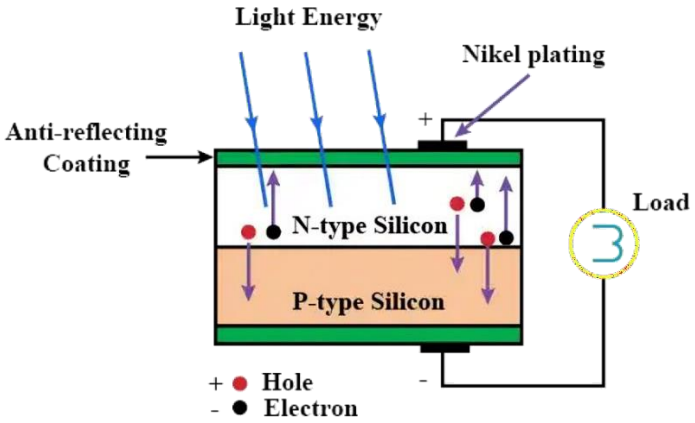

Fig. 2.2 Working principle of solar cell

2.2.3 Materials used in solar cell

The band gap of the materials utilized for this must be close to 1.5 eV. Typical materials include:

1. Silicon.
2. GaAs.
3. CdTe.
4. $CuInSe_2$.

2.2.4 Criteria for materials to be used in solar cell

These requirements must be met by any material used in a solar cell.

1. The band gap must be between 1eV and 1.8eV.

2. It must absorb light very well.

3. It must be able to carry electricity well.

4. As a last need, the raw material must be readily available and reasonably priced.

2.2.5 Advantages and Disadvantages of solar cell

While modern solar cells provide numerous benefits to individuals and businesses, they also have a few limitations. Solar cells benefit such as Non-polluting, Long-lasting, Maintenance-free. But its installation is very high, it gives low efficiency and during cloudy days and at night, solar energy cannot be generated, thus we cannot use it.

2.2.6 Efficiency, price, environmental impact of different generation solar cell

First generation solar cells had a lab-based efficiency of 24.7% and a module-based efficiency of 22.7%. Second generation solar cells have a lab-based efficiency of 18.4 percent and a module-based efficiency of 13.4%. Higher than 30% efficiency is common in 3rd generation solar cells. As shown in **Fig. 2.3**, 2nd generation solar cells per watt peak price and efficiency are cheaper compared to other generation technology. This is clearly illustrated. Solar cells from the third generation outperform those from the first generation in terms of efficiency and cost. Between 1977 and 2013, solar power's overall cost decreased by an incredible 99%.

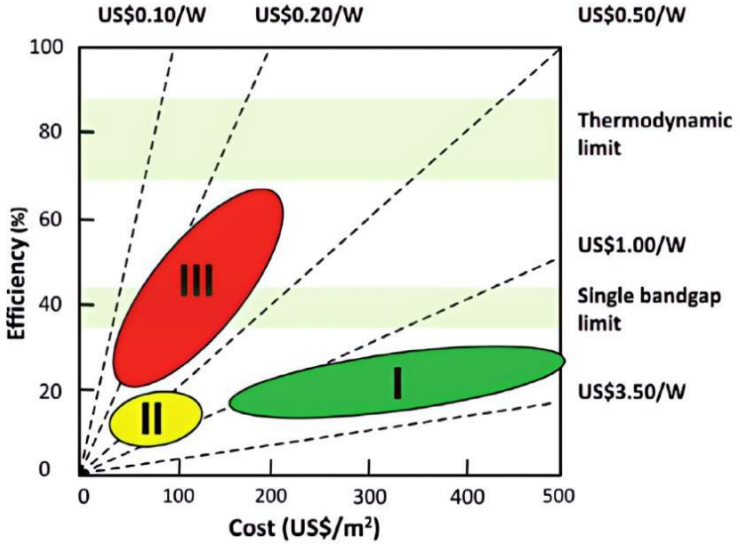

Fig. 2.3 Price vs efficiency among the different generation's solar cells.

Solar cell technology has always played an essential role in the development of green energy / sustainable energy. The manufacture of solar cells and their subsequent disposal have never been thought to be environmentally dangerous. This increase in pollution is a result of the solar cell manufacturing industry's recent rapid expansion. The PV manufacturing process includes the use of hazardous substances such as cadmium and arsenic. Vasilis Fthenakis, an environmental engineer at Brookhaven National Laboratory in Upton, N.Y., and his colleagues investigated the four most popular varieties of PV cells: multi-crystalline silicon, monocrystalline silicon, ribbon silicon, and thin-film silicon. (Alternatives like amorphous silicon and super-efficient multijunction cells were ruled out due to a lack of data or widespread use.) However inefficient thin-film solar cells may be, the energy required to purify silicon for alternative PV technologies still results in much lower emissions over the course of their whole life cycle than the fossil fuels required to create the same amount of electricity. Coal-burning power plants and other fossil fuels used to generate electricity for PV manufacturing facilities are the primary source of their pollution. A typical coal-fired power station emits about one kilogram (2.2 pounds) of greenhouse gases per kilowatt-hour of electricity, compared to just 55 grams (1.9 ounces) of global warming pollution per kilowatt-hour from monocrystalline silicate cells, the most energy-intensive to create. The overall harmful emissions from thin-film solar PVs are "90 to 300 times lower than those from coal power plants," according to experts in Environmental Science & Technology. As solar photovoltaics improve their effectiveness at converting sunlight into electricity or as the technology proves to last longer than the 30 years projected by manufacturers, the energy benefits will only improve. A lot longer than 30 years, argues Fthenakis: "There is no reason for this not to continue." A PV breeder cycle, in which electricity generated by solar panels is used to make additional solar cells, could make things even better for solar energy users. The area they have accessible [on] the roof and in the parking lot, according to Fthenaki, can easily meet 30% of the energy demand in [manufacturing] facilities [21].

2.2.7 Types of solar cell

Fig. 2.4 presents the categorization of the various photovoltaic cell technologies. In the industry, photovoltaic (PV) cell technologies are typically divided into three generations. This classification is typically determined by the fundamental material utilized and the level of commercial maturity.

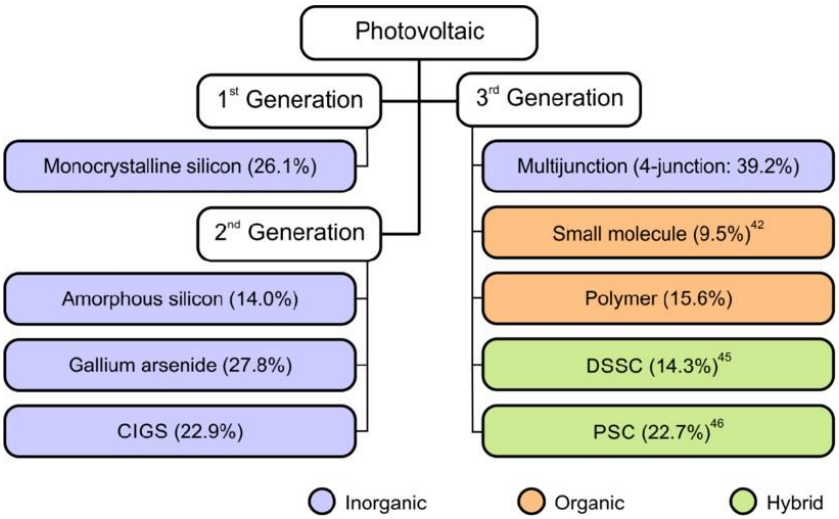

Fig. 2.4 Classification of PV cells

2.2.7.1 First-generation PV technologies: Crystalline silicon cells

The first silicon solar cell was invented by Bell Laboratories in 1954, with a 6% efficiency, and it was the first to be commercialized. The first commercial silicon conventional solar cells, which are constructed of silicon, are the most efficient for home usage and account for roughly 80% of all solar panels marketed worldwide. Single-cell silicon photovoltaic devices are the most efficient, and silicon is the second most common element on the planet, behind oxygen. With an energy band gap of 1.1eV, it's a semiconductor material well-suited to photovoltaics. There are three major varieties of crystalline silicon cells, each based on the process used to make the silicon wafers. Based on silicon type, there are three types:

- Monocrystalline (Mono c-Si)
- Polycrystalline (Poly c-Si)
- Amorphous Silicon Cells

Solar cells built from thin silicon wafers are the most common and efficient type of solar cell technology. Monocrystalline solar cells are the technical term for this type of solar cell. Commercial c-Si module production began in 1963, when Sharp Corporation of Japan began making commercial PV modules and constructed a 242-Watt (W) PV array (Green, 2001). They have a better efficiency (up to 26%) than other varieties of Solar PV, which means we may get more electricity from a given area of panel. As in silicon electronics, single crystal wafers are manufactured using the Czochralski method. It accounts for nearly a third of all sales. Due to the purifying process, single

crystalline silicon solar cells are more expensive to manufacture. Since single crystalline silicon is the most expensive, it is the most frequent form of silicon. Polycrystalline and amorphous silicon, on the other hand, are less pure. Polycrystalline solar panels are less expensive than monocrystalline solar panels because the silicon used to make them is manufactured in a different way. Instead of creating a single crystal, molten silicon is poured into a mold. Polycrystalline silicon cells have a maximum efficiency of 21%. Two layers of silicon are commonly found in silicon solar cells: a positive (p-type) layer and a negative layer (n-type). There are two ways to construct the positive layer: by doping silicon with boron and phosphorus, respectively, in order to create more holes and electrons in the lattice [19].

2.2.7.2 Second-generation PV technologies: Thin film solar cells

When compared to solar cells of the first generation made from silicon wafers, the vast majority of thin film solar cells and a-Si solar cells belong to the second generation of solar cells and have a lower price point. The light-absorbing layers in silicon-wafer cells can be up to 350 μm thick, but the light-absorbing layers in thin-film solar cells are typically only on the order of 1 μm thick. Solar cells that consist of thin films are characterized as;

- Amorphous silicon (a-Si).
- Cadmium-telluride (CdTe).
- Copper indium gallium de-selenide (CiGs).

In terms of mass production, the earliest solar cells made of amorphous silicon (a-Si) were the first. Low temperatures enable the production of amorphous (a-Si) solar cells, allowing flexible substrates such as polymer to be used. In terms of efficiency, these substrates are the best option. amorphous silicon (a-Si) solar cells are more common and less expensive. For solar cells, the term "amorphous" means the silicon material is non-crystalline or poorly structured and does not have a recognizable atomic lattice. The substrate/glass plate is covered with doped silicon. Reflecting side is dark brown, conducting side is silverfish. The efficiency and stability of a-Si solar cells are problematic. Cell efficiency decreases as the PV module level rises. PV module efficiencies range from 4% to 8% in the commercial market. They can work in hot weather and in regions with short days of sunlight [22]. The photovoltaic (PV) technique based on cadmium telluride (CdTe), a thin semiconductor layer designed to collect and convert sunlight into electricity, is known as cadmium telluride (CdTe)

photovoltaics. In multi-kilowatt systems, Cadmium telluride PV is the only thin film technology with lower costs than traditional silicon solar cells. For the most part, CdTe PV has a lower carbon footprint than other solar technologies, as well as the quickest payback period. Since CdTe has a payback time of less than a year, it allows for more rapid reductions in carbon dioxide emissions without creating immediate energy shortages. CdTe technology accounted for more than half of the thin film market in 2013 with a share of 5,1% of global PV production. First Solar, a firm situated in Tempe, Arizona, is a leading manufacturer of CdTe thin film technology. Cadmium is one of the most dangerous and deadly substances on the planet. In comparison to other Cd-based technologies, CdTe PV modules appear to be the most environmentally beneficial. CdTe safety is treated differently in China and Europe. In the EU, cadmium and its compounds are classified as carcinogens, but in China, rules only allow exports of Cd goods. Europe is now debating how to regulate the usage of Cadmium Telluride. Currently, the general consensus is that the use of Cadmium Telluride in residential and industrial rooftop installations does not offer a significant environmental risk [18]. In comparison to CdTe, CIGS is 10% to 12% more efficient. It's one of the most likely thin-film technologies because of its efficiency and cost. This material is prepared by sputtering, evaporating, electrochemically coating, printing and depositing with an electron beam [11]. Copper, indium, gallium, and selenide are deposited on glass or plastic, with front and rear electrodes to collect current, to make CIGS solar cells. In order to keep the material from absorbing too much sunlight, it needs a thinner layer. There are a number of thin-film photovoltaic (PV) materials to choose from. In the same way that these other materials may be placed on flexible substrates, so can CIGS layers.

2.2.7.3 Third-generation PV technologies

There has not yet been significant research conducted in the commercial sector on these potentially game-changing innovations. The majority of the solar cell types produced for the third generation are:

- Nano crystal based solar cells.
- Polymer based solar cells.
- Concentrated solar cells.
- Dye sensitized solar cells.

Solar cells based on nanocrystals, or quantum dots (QD), are also known as nanocrystal solar cells. A transition metal group of semiconductors is used to make solar cells. Crystals as small as a nanometer are referred to be "QD" materials, including porous Si or TiO2. Semiconducting nanocrystals are being created to take the place of silicon, cadmium telluride, and indium gallium telluride. Using this concept of a QD-based solar cell, a p-i-n solar cell in As/GaAs was designed Si is coated with nanocrystals that have been mixed in a bath. These crystals rapidly rotate and disperse as a result of centrifugal force. Compound semiconductor solar cells generate electron-hole pairs as a result of photons excitation of electrons. When a photon strikes a QD made of the same semiconductor material, there is a possibility that two or three electron-hole pairs will be created [23]. Polymer solar cells, also known as PSCs, have a polymer substrate, which makes them flexible. The very first PSC was developed by Tang et al. at the Kodak research lab. A PSC is distinguished by its many thin functional layers that are connected in succession on a polymer foil or ribbon. It is by utilizing a polymer donor and an acceptor (fullerene). Sunlight is absorbed by organic molecules such as conjugate polymers and conducting polymers. The development of conducting polymers earned Heeger, MacDiarmid, and Shirakawa the Nobel Prize in Chemistry in the year 2000. The photovoltaic effect is utilized by both PSCs and organic solar cells in order to convert electromagnetic radiation into electrical current. In order to develop the world's first polymer solar cell with a high power conversion efficiency, Yu et al. combined PPV, C60, and other derivatives. A brand new age in solar-powered polymer materials was ushered in by the use of this method. The researchers were able to boost the PPV PSC efficiency to 3.0 percent after making certain adjustments to the settings. The exceptional properties of PSCs made it possible to develop flexible solar devices, such as those made of textiles and fabrics. Increasing the functionality of liquid crystal displays can be accomplished with polarizing organic photovoltaics (ZOPVs) by making use of the same polarizer, a photovoltaic device, and sufficient light conditions or a solar panel [22]. Since the 1970s, the field of concentrating photovoltaics, often known as CPV, has been developed. It is the most recent advancement in solar cell technology. Concentrated cells are placed directly above PV solar cells and are used to collect solar energy in a condensed region. This technique makes use of huge mirrors and lenses to concentrate the light from the sun on a very small area that contains solar cells. The collision of individual rays of sunlight produces heat. A heat engine that is controlled by a power generator is driven by this heat energy. The future looks bright

for solar CPVs. It could be somewhat, highly, or not at all concentrated depending on the lens power. The solar cell efficiency of the concentrating photovoltaic approach is greater than forty percent, and it has no moving parts, no thermal bulk, and a quick response time [24]. Dye-sensitized solar cells, also known as dye-sensitized cells (DSC), are a type of photovoltaic (solar) cell that are considered to be of the third generation. These cells are able to convert any visible light into electrical energy. Due to the fact that it imitates the way in which nature absorbs light energy, this newly developed category of advanced solar cells has been compared to an artificial kind of photosynthesis.

2.2.8 Limitations of different generation solar cells

Generally, 1st generations solar cell based on Silicon (Si) solar cell. In spite of its high efficiency, the availability of silicon is complicated due to its expensive price. In addition, the silicon-based solar cell manufacture process is complicated. One of the most common reasons why solar cells don't work well is because their band gap is smaller than the amount of energy being absorbed by photons. The excess energy is dissipated as heat because the photons' energy exceeds the band gap. The open-circuit voltage is smaller than the band gap because the Fermi levels of both n-type and p-type silicon are always within the silicon band gap.

Thin-film solar cells are used in the second generation of solar cells. It has some advantages, such as a high absorption co-efficient. It is capable of occupying both vacuum and non-vacuum processes. Lower cost when compared to Si-based solar cells. Substrate at a low cost (Cu tape). It also has some drawbacks, such as the fact that in 2nd generation solar cells, environmental contamination begins during the manufacture process. Its ingredients are very difficult to come by.

The most recent solar cell technology is third generation solar cells. This form of solar cell is particularly beneficial since the raw ingredients for these solar cells are readily available, and the production method for these solar cells is simpler than for the other two technologies. This sort of solar cell is also inexpensive. It has certain advantages, but it also has some problems, like liquid electrolyte (low temperature), high cost, Ru (dye), and Pt (electrode) [19].

2.3 Dye-Sensitized Solar Cell (DSSC)

Dye-sensitized solar cells, also known as DSSCs, have emerged in recent years as an alternative to p-n junction photovoltaic systems that is both technically and economically viable. In the late 1960s, it was discovered that illuminated organic dyes can be used in electrochemical cells to produce electricity. This discovery took place in the late 1960s. The University of California at Berkeley performed an experiment on spinach to isolate chlorophyll, which is necessary for photosynthesis. When used in a DSSC, the absorption of light by a dye result in the generation of electrons. Dye-sensitized solar cells, also known as DSSCs, are a type of thin-film solar cell that has been the subject of a significant amount of research for more than two decades due to the fact that they are easy to produce, inexpensive, have a straightforward method of preparation, and have a low level of toxicity. However, there is a significant bit of space for improvement in the current DSSC materials due to the fact that they are expensive, there is a limited supply of them, and they are stable over the long term. Existing DSSCs have an efficiency of up to 12 percent, which can be achieved by using Ru(II) dyes and optimizing the material and structural properties of the device. Despite this, the efficiency of existing DSSCs is still lower than that of first- and second-generation solar cells, such as other thin-film solar cells and Si-based solar cells, which offer an efficiency of approximately 20–30 percent. Tithe dye is made up of a conjugated system (consisting of alternating single and double bonds), which is responsible for its ability to absorb light in the visible spectrum. When we looked at the many types of solar cells, we discovered that DSSC is one of the emerging materials for solar cells.

2.3.1 History of Dye-Sensitized Solar Cell (DSSC)

The DSSC is a photovoltaic device with a p-n junction. In DSSC, the light-absorbing sensitizer and the wide band gap semiconductor are integrated with the charge detachment and light absorption processes. Water may be split using TiO_2 with a small bias voltage and exposure to light in 1970, it was discovered [25]. In 1991, a cell combining nanoporous TiO_2 electrodes with a redox electrolyte based on the iodide/tri-iodide pair improved the conversion efficiency to 7%. These electrodes have a large active surface area. Ruthenium-based dyes and polymer gel electrolytes with good thermal stability were utilized in 2003, with a maximum efficiency improvement of 6%

[26]. In 2008, a redox electrolyte based on iodide produced an efficiency of 8%. [27]. The researchers made an effort to address the electrolyte's corrosive properties, which helped to increase photovoltaic efficiency and device stability by up to 11.5 percent [28]. Researchers have suggested the third generation of solar PV, which includes the quantum dot solar cell (10%), organic solar cell (11%) and DSSC (13%) in consideration of the disadvantages of the first and second generations of PV technologies. This third-generation technology can greatly reduce the cost of the device while optimizing efficiency.

Due to its incredibly affordable materials, mechanical flexibility, ease of fabrication and assembly, and environmental friendliness, DSSC has gained interest as a possible alternative to solar PV power. The most effective material for the DSSC's electron carrying material is thought to be a solar cell with a large band gap of 3.2eV for TiO_2. ZnO, while having a greater electron mobility and electron diffusion coefficient, is a strong rival of the TiO_2 photo anode. However, ZnO's conversion efficiency, which ranges from 0.4 to 5.8 percent, is lower than TiO_2's, which is 11 percent. While ZnO and TiO_2 have similar band gaps, electron transport durations, and dependence of light intensity, ZnO has a substantially longer electron lifespan than TiO_2 and a far lower "recombination rate" than TiO_2. Additionally, TiO_2 is more effective than ZnO. TiO_2 nanostructures, such as "nanoparticles," "nanorods," "nanowires," and "nanotubes," have been created (NTs). Sol-gel analysis, hydrothermal and solvothermal processes, chemical or physical vapor deposition methods, organic acid precursor methods, electrochemical deposition methods, etc. are some of the synthetic analysis techniques used to produce these TiO_2 structures.

Table 2.1 A comparison of Chemical, Electrical, Thermal, Mechanical and Optical Properties of TiO_2 and ZnO.

Properties		$\boldsymbol{TiO_2}$	$\boldsymbol{ZnO}$
Chemical Property	1.Crystal structure	Tetra gonal (Rutile Anatase, brookie)	Hexagonal (Rock Salt, Zinc Blende, Wurtize)
	2.Lattice Parameter	a= 0.3785 nm c= 0.951nm	a= 0.3249 nm c=0.52nm

	3.Band gap (ev)	3.2-3.59	3.2-3.3
Electrical property	4.Dielectric constant	114(Rutile)	8.5
	5.Electron effective mass (me)	9	0.24
	6.Electron diffusion coefficient [cm^2s^{-1}]	0.5(Bulk TiO_2), 10^8-10^4(np film)	5.2(Bulk ZnO)1.7×10^4(np film)
	7.Electron mobility Cm^2/Vs	Thin film :0.1-4.0	Thin film:205-300(Bulk ZnO)
Thermal Property	8.Thermal Conductivity ($Wm^{-1}k^{-1}$)	8.4	0.6,1-1.2
Mechanical Property	9. Density (g/cm^3)	3.79	5.606
	10. Melting point (C)	1875	1975
Optical Property	11. Refractive index	2.54	2

The features of TiO_2 nanostructures, specifically for DSSC, are discussed in **Table 2.1**. This will demonstrate how the use of photo electrode films containing TiO_2 nanoparticles can significantly improve the performance status of solar cells by delivering easily photo-excited electrons to transport paths away from directly impactful scattering centers, resulting in increased light-harvesting efficiency. The benefit of selecting TiO_2 np over ZnO as the working electrode encouraged me to continue trying to increase the conversion efficiency of dye-sensitized solar cells.

The development of solar cells is depicted in **Fig. 2.5**, where dye-sensitized solar cells are an optional way to Si-based solar cells and a promising photo electrochemical cell with an efficiency of up to 13%. However, despite sharing many of the same positive DSSC characteristics, the maximum conversion efficiency is lower than that of a silicon-based solar cell.

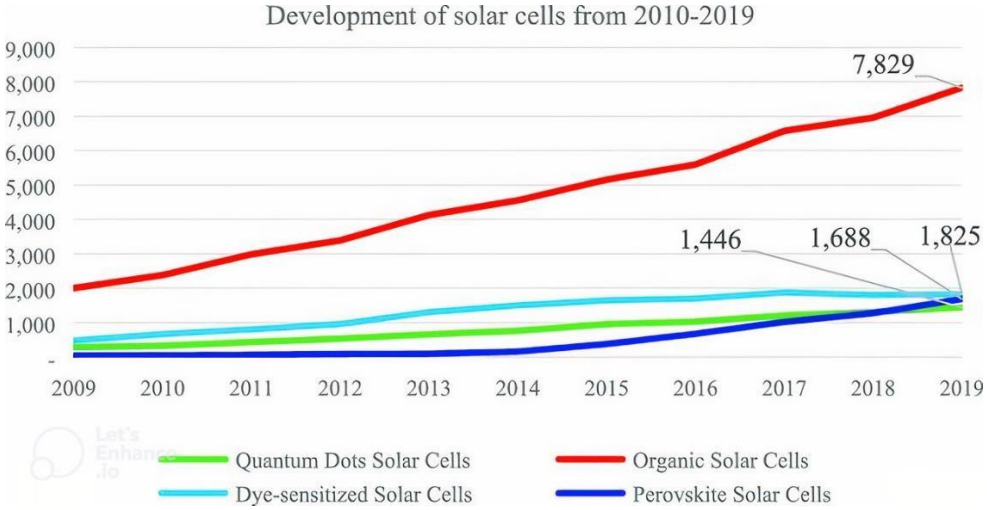

Fig. 2.5 Development of solar cell from 2010-2019 [10].

These nanoparticle films of titanium dioxide (TiO_2) are employed as photoelectrodes in DSSCs because of their chemical purity, surface area for dye absorption, and correct energy band. It is not possible for all photogenerated electrons to reach the collecting electrode because electron transport in a nano particle network occurs via a sequence of hops to neighboring particles. If the TiO_2 layer is thicker, the trapping mechanism may be less effective and produce more oxidized redox species. ZnO can be used as an option to solve the recombination problem. The high exciton binding energy makes it an excellent choice (60MeV). TiO_2 DSSCs, on the other hand, have a greater overall efficiency than ZnO DSSCs.

In comparison to TiO_2 DSSC, ZnO thin passivation shell layers have a lesser efficacy. For ZnO loss DSSC, dye absorption is the main problem. Carboxylic acid groups in the dyes lead to dissolution of zinc oxide and a perception of Zn^{2+} complex, resulting in decreased overall electron injection efficiency [27].

2.3.2 Factors affecting the efficiency of DSSC

DSSC efficiency is dependent on a number of things. Among them are:

- Working function and resistance of FTO.
- Semiconductor structure and carrier transport properties (oxide material).
- Absorption of wavelengths and alignment of the dye molecule-to-semiconductor-material contact.
- Transferring electrons from the Redox electrolyte to the stimulated dye molecule.

- The p^+ counter electrode's catalytic interaction with the iodic electrolyte.

2.4 Basic Structure of DSSC

To comprehend how the DSSC uses the sensitization of wide band gap semiconductors to convert light energy into electricity, it is important to have a solid understanding of the components of the device.

DSSC uses wide band gap semiconductors that have been sensitized to turn energy into electricity. The following are the fundamental elements of the DSSCs depicted in **Fig. 2.6**, all of which can be optimized to increase overall efficiency. The Fundamental Elements include:

1) Photo sensitizer / Dye
2) Electrolytes
3) Photo electrode
4) The counter electrode (CE)
5) Conductive glass substrate

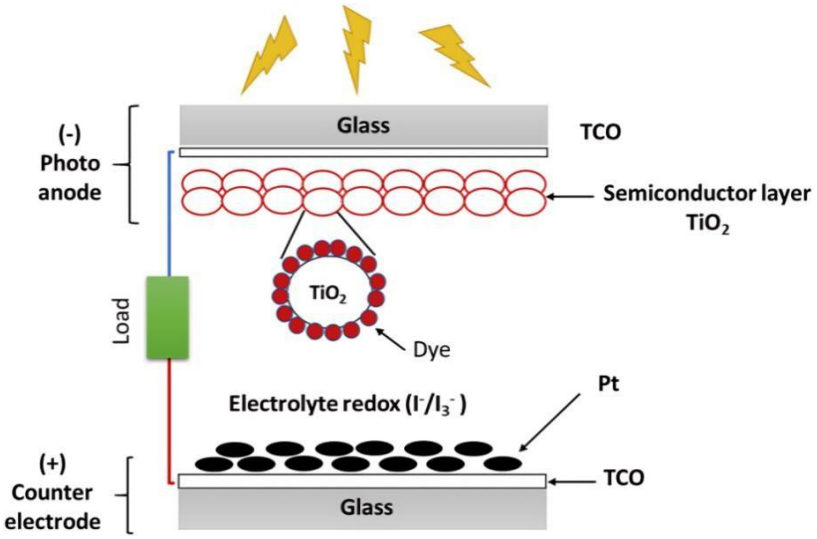

Fig. 2.6 Structure of DSSC.

2.4.1 Transparent substrate for both the conducting electrode and counter electrode

Clear glass substrates are frequently employed as substrates because they are very inexpensive, readily available, and possess great optical transparency in the visible and near infrared parts of the electromagnetic spectrum. On one side of the substrate, a conductive coating (film) is deposited, and it takes the form of a thin layer of transparent conductive oxide (TCO). The conductive film assures that the electric

resistance per square is kept to an absolute minimum. The value of such resistance is typically between 10 and 20 per square when it is measured at room temperature. On the conducting side is where the nanostructured wide bandgap oxide semiconductor, also known as the electron acceptor, is either coated, printed, or grown. In order to ease the mechanism of electron donation to the electrolyte, the counter electrode needs to be coated with a catalyzing layer prior to the assembly of the cell. This layer can be graphite, for example (electron donor). It is important to keep in mind that after being coated with the conductive film, the transparent conducting electrode's transparency levels do not reach 100 percent across the full visible and near infrared (NIR) section of the sun spectrum. This is something that one must keep in mind. The fact that nanostructured material is deposited on an electrode makes it less transparent is a well-known concept. A typical transmittance measurement (conducted with the use of a dual beam spectrophotometer) is depicted in **Fig. 2.7** for a conductive glass electrode both before to and following its coating with a nanostructured TiO_2 layer [18].

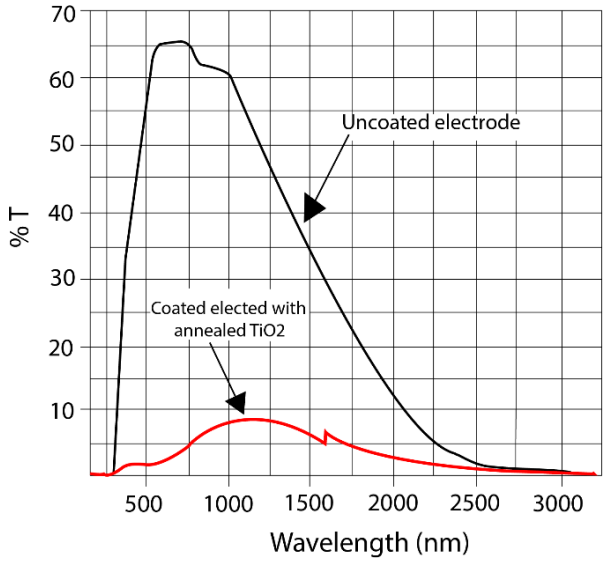

Fig. 2.7 Transmittance of conductive glass electrode before and after being coated with nanostructured TiO_2 layer.

2.4.2 Nanostructured wide band gap semiconducting layer

A ZrO_2 surface passivated ZnO/TiO_2 hydrated transparent solution was spin coated on a pre-cleaned circular area of approximately 0.25 cm^2 FTO-coated glass at 3000 rpm for 20 s to construct the photoanode with a compact under-layer. A 2 mL vial of deionized water was filled halfway with ZnO/TiO_2 surface passivated hydrated ZrO_2 powder, and the solution was sonicated until it turned translucent. As a final step, the vial was treated with another drop of Triton X-200 before being subjected to another round of ultrasonic cleaning for a total of 20 minutes. The compact layers were gently cured for 10 minutes at 240 ℃ between spin coats, then allowed to cool to room temperature naturally. The structural integrity of the compact layer and the stability of subsequent processing are dependent on the slow heat curing process. In order to get the necessary coating thickness, this process was repeated a number of times. After that, the compact films were sintered at 450 ℃ for 30 minutes before being allowed to cool to ambient temperature to complete the process. The pastes were made in two stages for thick paste formation. The citric acid and ethylene glycol mixture was heated to 70 °C under steady stirring until a clear solution was achieved. Citric acid solution was added to the mortar and pestle to generate a smooth colloidal paste with a long shelf life from 0.6 g of ZnO/TiO_2 surface passivated ZrO_2 powder. It was then spun-coated on the top of the compact layer three times to achieve the appropriate film thickness. A 450 ℃ muffle furnace was used to sinter the films, which were allowed to cool to ambient temperature after 30 minutes [23].

2.4.3 Photo sensitizer / Dye

Dye plays crucial roles in the absorption and conversion of solar radiation to electricity. A highly effective photo-sensitizer must be fabricated in accordance with the following specifications:

- The dye must be luminous.
- The dye's absorption spectrum needs to cover the ultraviolet-visible and near-infrared ranges.
- The dye must have a high visible light-harvesting capacity.
- The efficiency with which electrons are injected into a semiconductor is referred to as the conduction band.

- High rates of electron transport are ensured by *-O* or *-OH* groups that have the ability to anchor to the TiO_2 surface.

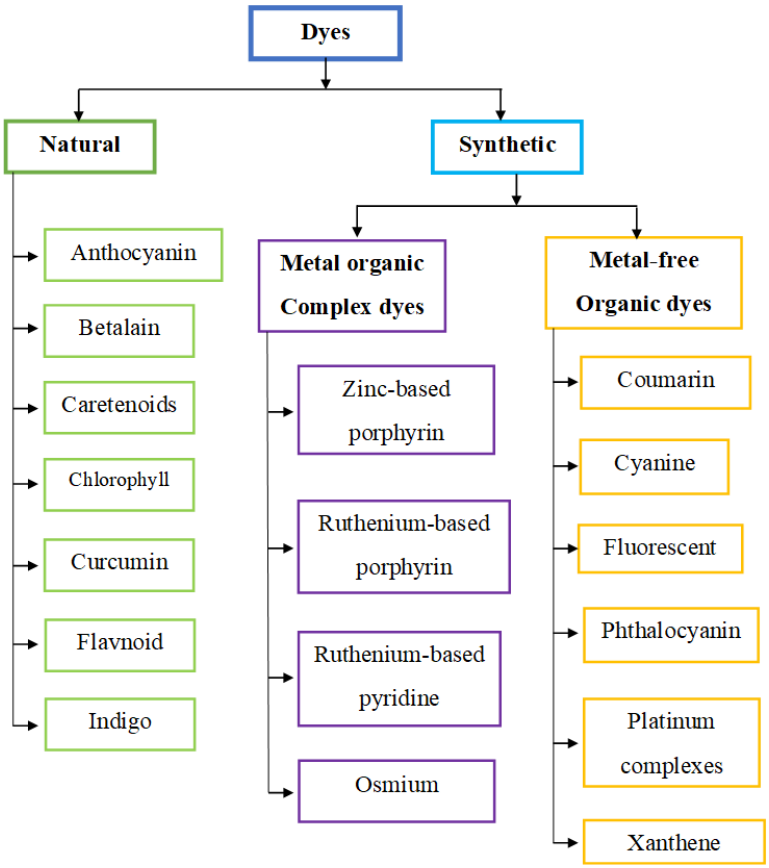

Fig. 2.8 Categories of common dyes used in DSSC with example [30].

Ru complex's photo sensitizers (N 719) for dye-based DSSC demonstrate the maximum efficiency of 11.2 percent, according to Gratzel and his group's research [25]. Ru complex has a high visible light-harvesting capacity, excellent chemical stability, and the possibility of exchanging charge with semiconductor materials. This is due to the fact that the absorption spectra of Ru complex dye cover the ultra violet, visible, and near infrared regions. In **Fig. 2.8**, the common types of DSSC dyes are shown.

2.4.4 Electrolytes

The presence of a redox mediator in the electrolytes facilitates the transfer of charge between the photo electrode and the counter electrode. An electrolyte, such as I^-/I_3^-, is made up of five primary components: 1) a redox pair; 2) a solvent; 3) additives; 4) cations; and 5) ionic liquids [32], [34].

For the regeneration of dye and electrolyte, it is important to take into account the redox potential of the iodide and tri-iodide. Iodide and tri-iodide have proven to be an effective redox couple for usage in DSSC. A redox electrolyte is comprised of iodide, iodides, and perhaps additional additives as well.

In DSSC, the electrolyte can be one of three different types depending on the solvent that was used to prepare it. The terms "Aqueous Electrolyte," "organic Solvents-based Electrolytes," and "Ionic Liquids-based Electrolytes" are used to describe these substances. Ionic liquids give good ionic conductivity as well as long-term thermal and chemical stability. In spite of the fact that I/I electrolyte erodes glass/ TiO_2/Pt, it has been demonstrated that I^-/I_3^- is an extremely efficient electrolyte [35], [36].

2.4.5 Photo-Electrode / Working Electrode

In direct semiconductor solar cells (DSSC), the TCO glass substrate electrode, also known as the working electrode, is formed by depositing a thin film layer of nanostructured semiconductor material on top of a fluorine-doped tin oxide (FTO). TiO_2, Nb_2O_5, ZnO, SnO_2 (n-type), and NiO (p-type) are some examples of sample conductor materials that are utilized for it. TiO_2 is one of the most extensively utilized of these since it is non-toxic, has a lower cost, and is an abundant material, which means it is easy to obtain. The size of the interconnected nanoparticles in the generated porous electrode film varied from 15 to 30 nm, and the electrode itself appeared as a transparent porous electrode film. The thickness of the film ranged from 10 micrometers to 15 micrometers.

As a deposition process for film preparation, screen printing and the doctors' blade approach are both being utilized at this time. These two processes both involve the deposition of viscous TiO_2 paste, which is then used to coat the substrate. The coating process is called "viscous TiO_2 paste coating." After the screen printing and doctors blade method for deposition of viscous colloidal TiO_2 on a substrate has been done, the next step is the sintering, which is carried out at (450-500) ℃ [29]. This is done after the combustion that removes the binder metal oxide (TiO_2) paste onto the substrate. As a photo anode or working electrode, TiO_2 is the best semiconductor since it possesses both high efficiency and stability. ZnO also demonstrates superior photo anode efficiency, which may be due to the fact that its band gap is comparable to that of TiO_2.

2.5 Working Principle of Dye-sensitized solar cells

Having a solar cell that is dye-sensitized is known as a dye-sensitized solar cell. "Dye" means something that reacts to light. Processes such as "light absorption," "charge separation," and "charge collecting" are all part of the DSSC's operation. **Fig. 2.9** shows a simplified flow chart illustrating the DSSC's operation:

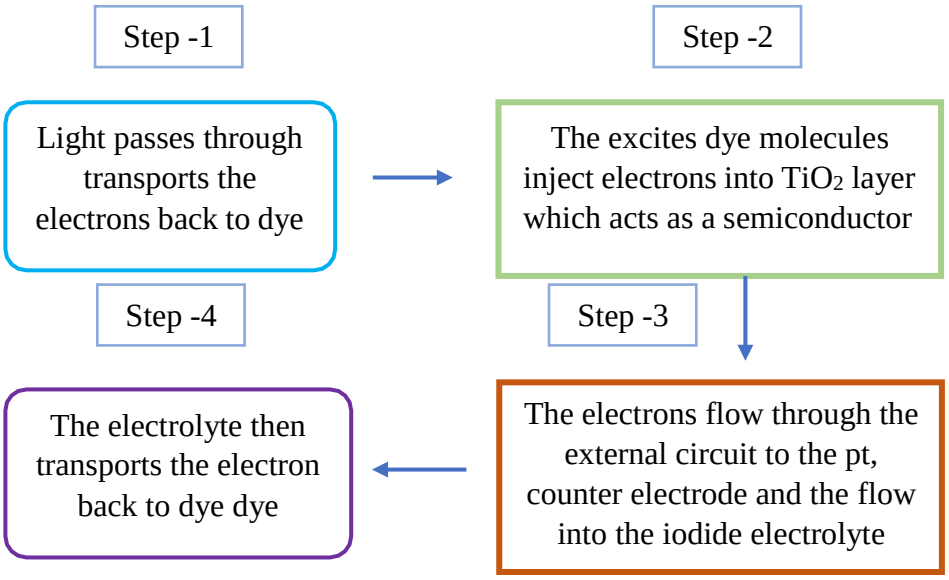

Fig. 2.9 Flow chart of basic Working principle of DSSC.

2.6 Performance analysis of DSSC

The increased demand for renewable energy is directly correlated to the expanding global population. Silicon solar cells have become increasingly popular as traditional forms of energy generation, such as fossil fuels and nuclear power, have become less viable [30]. Solar energy is the most plentiful and limitless source of energy. Dye-sensitized solar cells, also known as DSSCs, are regarded to have a substantial amount of potential in the field of photovoltaics [31]. This is due to the simple production method that can be used and the inexpensive cost. Numerous synthesis procedures have been applied in the quest to successfully create nonporous TiO_2 in the anatase phase. The sol-gel, hydrothermal, and solution combustion synthesis techniques are among the most common and straightforward of these approaches [38], [39].

A photovoltaic device must continue to function normally for a period of forty years even if its performance suffers significantly. Therefore, the conductivity of each

component of nano crystalline injection solar cells, such as the conducting glass, the TiO_2 layer, the sensitizer, the electrolyte, the counter electrode, and the sealant, has been thoroughly analyzed. Because the TCO glass and the Nano crystalline TiO_2 layer are undeniably stable, the focus of the research has been placed on the four additional components [40]. The current density of the TiO_2 nanoparticle-based dye-sensitized solar cell was greater when compared to the TiO_2-ZnO Nano composite-based dye-sensitized solar cell [37]. TiO_2 nanoparticles are extremely small. TiO2 nanoparticles in their anatase phase have been found to have potential for use in DSSC applications [41]. This phase has a bandwidth of 3.2 eV. In addition, in comparison to TiO_2 nanoparticles, ZnO nanoparticles have a larger excitonic electron mobility of roughly 115 cm^2/V.S and a bandwidth that is 3.3eV wider. [40] Chung et al. reported used solution combustion synthesis to manufacture TiO_2 Nano particles with a specific surface area of 47 m^2/g, which were used in the manufacturing of DSSC [38]. This method was used to produce the powders. TiO_2 nanorods were created using a hydrothermal process by Govindaraj et al., and these nanorods were used as photoanodes in a DSSC, where they achieved an efficiency of 5.42 percent [39]. A mechanochemical technique was employed by Wahyuningsih et al. to generate a TiO_2 NRs-ZnO composite, and then they used it as a photoanode in a DSSC efficiency of 0.85% [37]. Nanostructured TiO_2 was produced by Myrsini Giannouli and colleagues, who then used it as a photo anode in a DSSC that had an efficiency of 0.39 percent.

The efficiency of converting photon energy into electrical energy can be stated as follows for solar spectrum radiation with photon flux:

$$\eta = \frac{J_{sc} \times V_{oc} \times FF}{J_0}$$

Here

J_{sc} = Short Circuit Current.

V_{oc} = Open Circuit Voltage

J_0 = Photon Flux

FF = Fill Factor

In another way, kind find the performance. It is evaluated by power conversion efficiencies (PCE), Short-circuit current density, open-circuit voltage (V_{oc}), maximum power output [P_{max}], series and shunt resistance, incident photon conversion efficiency (IPCE) and Fill Factor (FF),

Table 2.2: Different kind of dye for power conversion efficiency (PCE) were calculated

TiO_2 Nanostructure	Compounds	PCE (%)
Nanoparticles/ Nanotubes	N719 + AC-9 + CDCA	6.97
	N719 + AC-9	6.48
	AC-9	4.56
	N719	5.56
Nanoparticles/ Nanowires	N719 + AC-9 + CDCA	5.44
	N719 + AC-9	4.9
	AC-9	2.5
	N719	4.15
Nanoparticles	N719 + AC-9 + CDCA	6.69
	N719 + AC-9	6.1
	AC-9	4.21
	N719	5.1

Considering the tiny mistakes that show that the manufactured cells are very repeatable, just one device per type was produced with TiO_2 nanotubes and nanowire [45].

2.7 Fabrication of DSSC

Afterward, the ZnO films were washed and rinsed in ethanol, acetonitrile, and dried in the air at room temperature for a total of 12 hours. Two electrode DSSCs with an active area of 0.25 cm^2 have been constructed utilizing a conventional two-electrode arrangement. As photoelectrodes, we employed dye-loaded ZO_{50}, ZO_{100}, ZO_{150}, and ZO_{200} samples, and as counter electrodes, we used platinum-coated FTO. The counter electrode is made using a simple drop cast process, employing the 10 mM $H_2PtC_{l6}.6H_2O$ in 2-propanol solution on the pre-drilled FTO and annealing at 723 K for 10 minutes. A thermoplastic was used to assemble the two electrodes (1 mm). A predrilled hole in the counter electrode is used to fill the gap between the electrodes

with an electrolyte containing 0.1 M lithium iodide and 0.05 M iodine in acetonitrile.[46]

2.8 Advantages and Disadvantage of DSSCs

Dye-sensitized solar cells (DSSCs), commonly referred to as Gratzel cells, are one of the most recent developments in thin-film solar cell technology. These photovoltaic cells offer a variety of benefits, but they also have a few drawbacks. The following is a list of some of the benefits and drawbacks associated with DSSCs:

- In comparison to regular silicon-based panels, they absorb more sunlight per square inch of surface area, making them the most efficient third-generation solar technology currently available.
- Low density applications like rooftop solar collectors, where the light weight and mechanical durability of the printable cell is a significant benefit are viable replacements for present technology [44].
- The high-efficiency, high-cost cells may be better appropriate for large-scale installations. If the DSSC's efficiency improves even somewhat in the future, it might be acceptable for some of these uses.
- DSSCs are able to operate in low light settings, such as clouded skies and indirect sunlight.
- They are inexpensive, simple to make, and made from readily available and long-lasting raw components.
- The DSSC's mechanical toughness contributes to improved efficiency at a wide range of temperatures.
- There are two ways to build an efficient DSSC: one is to use a conductive plastic top layer and the other is to use a non-conductive plastic top layer
- When it comes to large-scale deployments, the DSSC is not a viable solution because of its high cost and low efficiency. DSSC has not yet been produced on a large scale commercially. Because of the dramatic decrease in the cost of silicon solar panels, other forms of solar technology, such as solar thermal and thin film, have fallen by the wayside [42].
- It is important to keep in mind that the liquid electrolyte used in dye-sensitized solar cells is not temperature stable. At low temperatures, the electrolyte can

freeze, resulting in a loss of power and causing harm. When the temperature rises, the work of sealing the panels becomes more difficult.

- The electrolyte solution, which contains volatile organic solvents and must be sealed with care, is another big problem. Solid electrolyte replacement has been a primary focus of research for some time.

2.9 Zinc oxide

An inorganic substance having the formula ZnO, flowers of zinc may be a mineral. philosopher's wool (ZnO) may be a white powder that can't be dissolved in water, and it's widely used as an additive in an exceedingly big variety of materials and products like rubbers and plastics also as cement, ceramics, glass and other building materials, paints, ointments and other cosmetics similarly as batteries, ferrites, fire retardants and first-aid tapes [45]. although zincite, the mineral that contains flowers of zinc, may be a present occurrence, the bulk of oxide is manufactured synthetically. ZnO is an II-VI semiconductor with a broad bandgap. because of the presence of oxygen vacancies or Zinc interstitials, the semiconductor is n-type by default. This semiconductor possesses a large bandgap, good transparency, high electron mobility, and a powerful room-temperature luminescence, among other beneficial features. Transparent electrodes in liquid displays, energy-saving or heat-protecting windows, and electronic devices like thin-film transistors and light-emitting diodes can all have the benefit of these qualities.[47]

2.9.1 Crystal structure of ZnO

Crystalline Under standard laboratory settings, the crystal structure of ZnO is wurtzite (B4). The structure of ZnO wurtzite is characterized by a hexagonal unit, two lattice parameters remarked as a and c, and membership in either the C_{46V} or $P6_{3mc}$ space group. **Fig. 2.10** demonstrates quite clearly that the structure is formed from two interpenetrating hexagonal closed packed (hcp) sublattices. These sublattices each encompass one style of atom (either Zn or O), and that they are displaced with reference to one another along the threefold c-axis. it's possible to produce a simple explanation for it by way of a schematic representation. This representation is of variety of alternate planes that are layered layer-by-layer along the c-axis direction. These planes are composed of tetrahedrally coordinated Zn^{2+} and O^{2-}. ZnO's non-centrosymmetric structure is that the results of the tetrahedral coordination of its crystal

structure. Because each anion in wurtzite hexagonal ZnO is surrounded by four cations at the corners of the tetrahedron, the structure displays tetrahedral coordination and, as a result, sp3 covalent bonding [48].

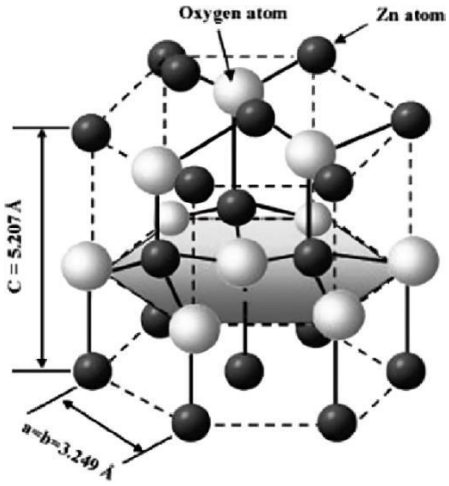

Fig. 2.10 The hexagonal wurtzite structure model of ZnO. The tetrahedral coordination of Zn-O is shown. O atoms are shown as larger white spheres while the Zn atoms are smaller brown spheres

2.9.2 Chemical properties

ZnO in its purest form is a white powder, but in nature it can only be found as the extremely uncommon mineral zincite, which typically has manganese and other impurities that give it a color ranging from yellow to red. When heated in air, crystalline zinc oxide undergoes a thermochromic transformation, going from white to yellow, and then back to white after it has cooled. This color change is produced by a slight loss of oxygen to the environment at high temperatures, which forms the non-stoichiometric $Zn_{1+x}O$ compound. At 800 °C, x = 0.00007, so the compound is non-stoichiometric. An example of an amphoteric oxide is zinc oxide. It is extremely difficult to dissolve in water, although it is possible to do so in most acids, including hydrochloric acid:

$$ZnO + 2\ HCl \rightarrow ZnCl_2 + H_2O$$

Solid zinc oxide will also dissolve in alkalis to give soluble zincates:

$$ZnO + 2\ NaOH + H_2O \rightarrow Na_2[Zn(OH)_4]$$

ZnO undergoes a gradual reaction with the fatty acids present in oils, which results in the production of the corresponding carboxylates, such as oleate or stearate. When ZnO is combined with a concentrated aqueous solution of zinc chloride, products resembling cement are produced. These cement-like substances are known scientifically as zinc hydroxy chlorides. Dentistry was one of the applications for this cement. When ZnO is treated with phosphoric acid, a substance that is similar to cement is formed. Materials that are similar to this are utilized in dentistry. Hopeite, also known as $Zn_3(PO_4)_2.4H_2O$, is one of the primary components of the zinc phosphate cement that is generated as a result of this reaction. At temperatures approximately 1975 °C with a constant oxygen pressure, ZnO breaks down into zinc vapor and oxygen. During a carbothermic reaction, the oxide is converted into zinc vapor at a significantly lower temperature (about 950 °C). This occurs when the oxide is heated with carbon.

$$ZnO + C \rightarrow Zn(_{Vapor}) + CO$$

When heated, zinc oxide has the potential to cause a strong reaction with aluminum and magnesium powders, as well as chlorinated rubber and linseed oil, which poses a risk of fire and explosion. Zinc sulfide is produced when it is brought into contact with hydrogen sulfide. This reaction is applied in the business world.

$$ZnO + H_2S \rightarrow ZnS + H_2O$$

2.9.3 Physical properties

Hexagonal wurtzite and cubic zincblende are the two primary crystal kinds of oxide showing in **Fig. 2.11**. The wurtzite structure is that the foremost frequent and most stable under ambient circumstances. A cubic lattice structure could also be accustomed stabilize the zincblende form by growing ZnO on the substrate. Zinc and its oxide centers are both tetrahedral, which is that the foremost common Zn geometry (II). to transform into rocksalt, ZnO must be under high pressures of around 10 GPa.

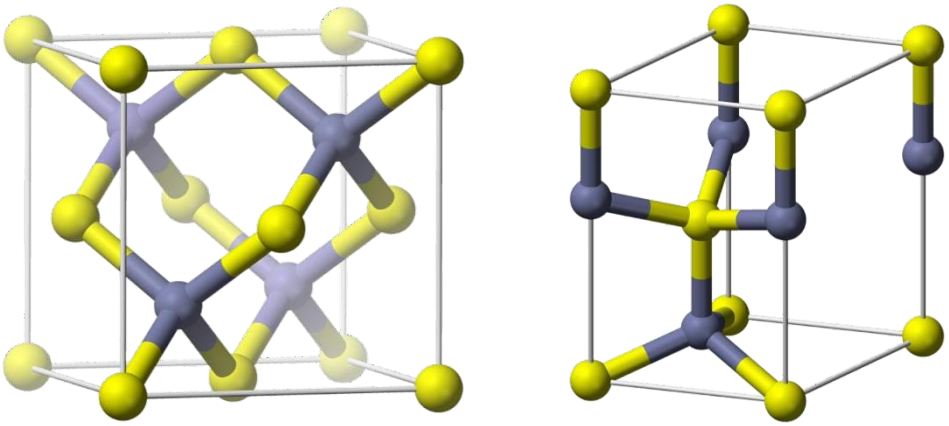

(a) **(b)**

Fig. 2.11: (a) A zinc blende unit cell **(b)** Wurtzite unit cell

There is no inversion symmetry within the polymorphs of hexagonal and zincblende (reflection of a crystal relative to any given point doesn't transform it into itself). Hexagonal and zincblende ZnO have piezoelectricity, while hexagonal ZnO exhibits pyroelectricity thanks to these and other lattice symmetry features. C_{6v} (Schoenflies notation) or $P6_{3mc}$ (Hermann-Mauguin notation) is that the space group of the hexagonal structure. For hexagonal cells, the optimum value of the lattice constants is about 1.60, and so the lattice constants for this method are 3.25 Å and 5.2 Å. ZnO's bonding is predominantly ionic (Zn^{2+} –O^{2-}) with radii of 0.074 nm for Zn^{2+} and 0.140 nm for O^{2-} , like most group II-VI materials. ZnO's high piezoelectricity and preference for the wurtzite structure over the blende structure are both due to this characteristic. Zinc and oxygen planes are electrically charged as a result of the polar Zn-O bonds. ZnO's surfaces are atomically flat, stable, and exhibit no reconstruction to stay up electrical neutrality compared to other materials. ZnO's oddity has yet to be fully understood. according to these investigations, ZnO wurtzite surfaces were found to be flat and there was no reconstruction on them. Wurtzoid structures were accustomed explain the origin of ZnO flatness and also the absence of reconstruction.

2.9.4 Mechanical properties

On the Mohs scale, ZnO registers an estimated hardness of 4.5, which places it within the softer end of the spectrum. Its elastic constants are not up to those of relevant III-V semiconductors like GaN. These lower constants are a result of its smaller size. Ceramics can enjoy ZnO's high melting temperature, moreover as its high heat capacity and warmth conductivity, low thermal expansion, and low thermal expansion rate. At a

temperature of 10 K, the E2 optical phonon in ZnO contains a lifespan that's exceptionally high at 133 ps. it's been asserted that ZnO, out of all the tetrahedrally linked semiconductors, possesses the most important piezoelectric tensor, or at the very least, one that's admire that of GaN and AlN. It's a fabric of great technological importance for a large style of piezoelectrical applications, all of which elicit a considerable electromechanical coupling.

2.9.5 Electrical properties

ZnO incorporates a direct band gap that's measured at 3.3 eV when the fabric is at normal temperature. There are many benefits that come together with having an outsized band gap, like greater breakdown voltages, the flexibility to take care of large electric fields, less electronic noise, and therefore the capability to work at high temperatures and high powers. By alloying ZnO with mineral or cadmium oxide, the bandgap of the fabric is further adjusted to be between 3 and 4 eV. Even within the absence of deliberate doping, the overwhelming majority of ZnO possesses n-type character. In most cases, the origin of n-type character is also traced back to a nonstoichiometric process; yet, the controversy surrounding this subject continues. On the idea of theoretical computations, an alternate hypothesis has been advises suggesting that inadvertent substitutional hydrogen impurities are guilty. By exchanging Zn with group-III elements like Al, Ga, or In, or by substituting oxygen with group-VII elements chlorine or iodine, it's simple to supply controllable n-type doping. Doping ZnO to a p-type state that's reliable continues to be challenging. This issue arises as a result of the limited solubility of p-type dopants and also the plentiful n-type impurities that serve to catch up on this shortcoming. Both GaN and ZnSe are shown to possess this issue. The inhomogeneity of the samples makes the measurement of p-type un "intrinsically" n-type material harder than it'd well be. Dopants of the p-type are identified because the elements Li, Na, and K from Group I; the weather N, P, and As from Group V; yet as copper and silver. At temperature, many of them, however, form deep acceptors and don't cause considerable p-type conduction. The temperature features a significant impact on the electron mobility of ZnO, which reaches its highest value of 2000 $cm^2/(Vs)$ at 80 K. There are only a few data available on hole mobility, with values starting from 5.0 to 30.0 $cm^2/(Vs)$. ZnO discs, which perform the function of a varistor, are the active material within the overwhelming majority of surge arresters [49]

2.9.6 Application of ZnO

ZnO's unique properties can be used in a variety of ways. Since ZnO has such a large band gap, it can form clusters of ZnO nanocrystals and nanowires. Synthesis of P–N homojunctions has also been reported in several literatures due to the large band gap. ZnO has a free-exciton binding energy of 60 meV, which makes it possible to manufacture many fine optical devices at room temperature and much higher. Non-linear optical devices can benefit from ZnO crystals and thin films' second- and third-order nonlinear optical properties. Zinc oxide's ability to control its physical properties is a major factor in the development of smart application devices [19]. It is possible to fine-tune the electrical, optical, magnetic, and chemical properties of cations and anions with mixed valence states and deficiencies by permuting and combining their two primary structural characteristics (vacancies) [50]. ZnO has a wide range of uses, as shown in the following figure (**Fig. 2.12**):

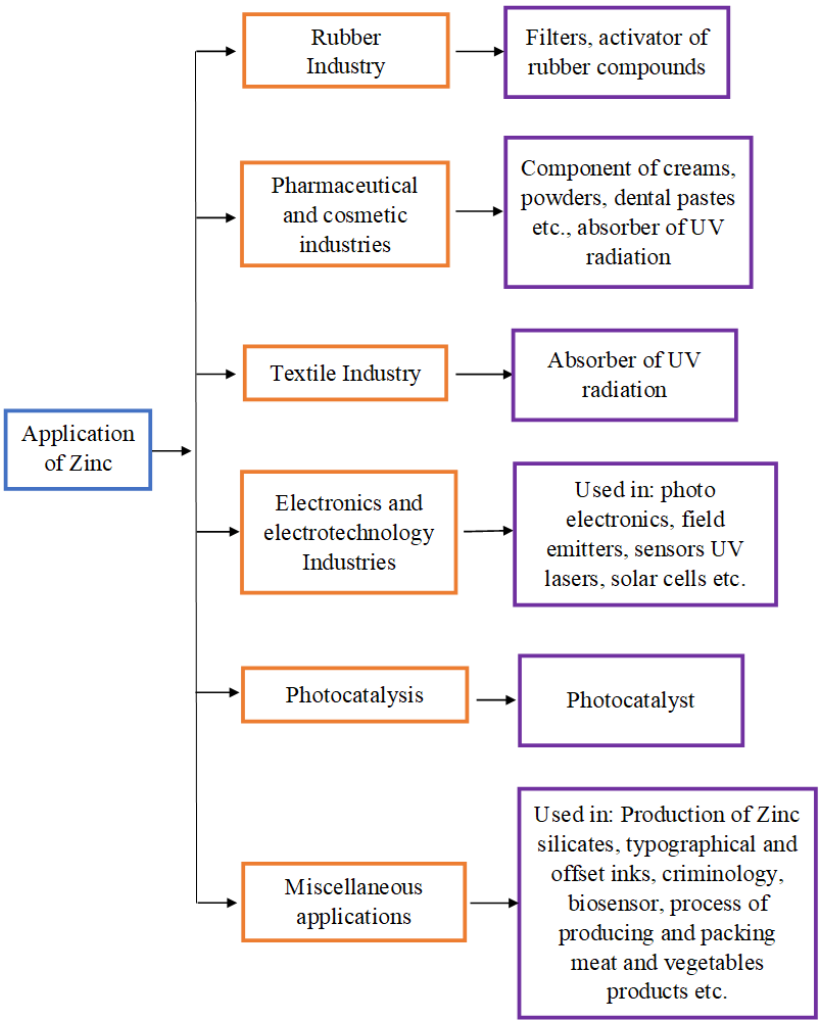

Fig. 2.12 Schematic representation of the ZnO application

2.9.7 Future of zinc oxide

High-quality Zinc Oxide's future is sure to be interesting. Non-medicinal applications may see advancements that outpace those now being used in medicine. One should expect to see a lot of progress in Zinc Oxide Nanorod Sensors, Spintronics, and Piezoelectricity in the near future [51].

CHAPTER 3

PARAMETER DESCRIPTION

3.1 Introduction

Throughout this chapter, we will talk about a variety of parameters (such as saturation current, series resistance, shunt resistance, ideality factor, barrier height etc.,). And how the various parameters influence the performance of the DSSC.

3.2 Saturation current

A diode's reverse saturation current (or scale current) is the reverse current created by the diffusion of minority carriers from the neutral regions to the depletion zone. This is known as reverse saturation current. The reverse voltage has essentially no effect on this current.

For an ideal p-n diode, Is, the reverse bias saturation current, is calculated as follows:

$$I_s = eAn_i^2\left(\frac{1}{N_D}\sqrt{\frac{\overline{D_P}}{r_p}} + \frac{1}{N_A}\sqrt{\frac{\overline{D_n}}{r_n}}\right) \quad \text{.....} \quad (3.1)$$

Where,

e is elementary charge

A is the cross-sectional area

D_P, D_n, are the diffusion coefficients of holes and electrons, respectively,

N_D, N_A are the donor and acceptor concentrations at the n side and p side, respectively,

n_i is the intrinsic carrier concentration in the semiconductor material,

r_p, r_n are the carrier lifetimes of holes and electrons, respectively.

The bulk of charge carriers cannot diffuse across the junction when the reverse bias is increased. However, certain minority charge carriers are able to traverse the junction due to this potential. n- and p-region minority charge carriers are temperature-dependent and independent of the applied bias voltage because they are formed by electron-hole pairs that are thermally generated. Due to the moment of majority charge carriers, the applied

bias voltage works as a forward bias voltage for these minority charge carriers, causing a small external circuit current to flow in the opposite direction of the conventional current. When analyzing a diode's temperature coefficient, it is important to keep in mind that the saturation current is not a constant for any given device; rather, it changes with temperature. For every ten degrees Celsius increase in temperature, it is said to grow by twice [53]. A p-n junction solar cell's saturation current (I_0) is an indicator of the cell's quality. Dark current-voltage measurements are commonly used to estimate this parameter [54].

3.3 Series resistance

There are three factors that contribute to the development of series resistance in a solar cell: first, the flow of current through the solar cell's emitter and base; second, the resistance of the contact between the metal contact and the silicon; and third, the resistance of the top and rear metal contacts [52]. The primary effect of series resistance is a decrease in the fill factor; however, extremely high values may also have the effect of diminishing the short-circuit current.

$$I = I_L - I_0 \exp\left[\frac{q(V + IR_s}{nKT}\right] \quad (3.2)$$

Here, I stands for the output current of the cell, I_L for the light generated current, V for the voltage across its terminals, T for the temperature, and constants q and K for the ideality factor. It is necessary to use numerical methods to calculate an implicit function like the one in this formula, which appears on both sides of the equation as current, I. In **Fig. 3.1**, a series resistance diagram is depicted. In **Fig. 3.2**, the *I-V* curve can be seen to be affected by the series resistance.

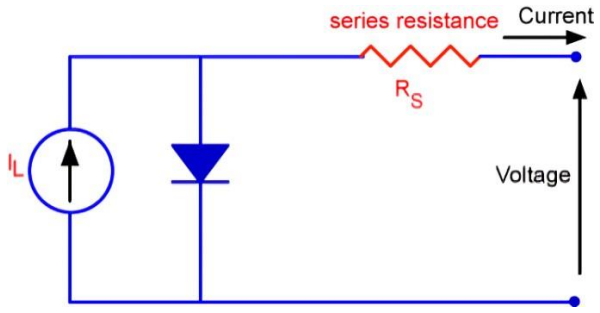

Fig. 3.1 Schematic of a solar cell with series resistance

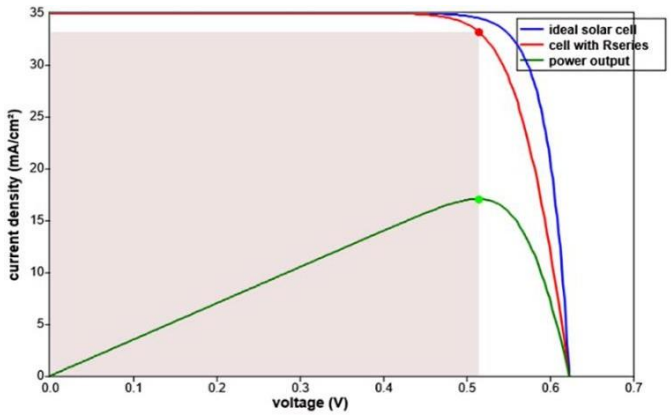

Fig. 3.2 Effect of series resistance on *I-V* curve

Because the size of the solar cell is 1 cm^2, the units of resistance can be either ohm or ohm cm^2; nevertheless, the more common unit is the ohm. Until it becomes extremely large, the series resistance has no effect on the short circuit current (also known as ISC). At open-circuit voltage, the series resistance does not have any impact on the solar cell since there is no overall current flow through the solar cell, and as a result, there is no current flow through the series resistance. However, the series resistance has a significant impact on the *I-V* curve as it gets closer and closer to the open-circuit voltage. Finding the slope of the current-voltage curve at the point where the open-circuit voltage is measured is a straightforward approach for determining the series resistance produced by a solar cell [56].

3.4 Shunt resistance

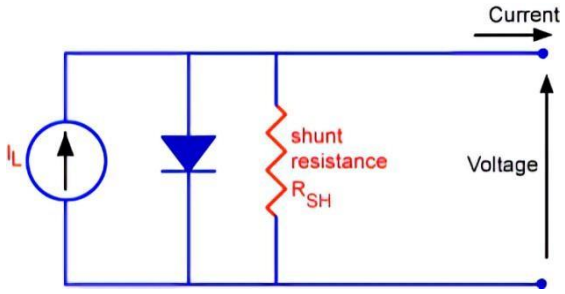

Fig. 3.3 Circuit diagram of a solar cell with shunt resistance

$$I = I_L - I_0 \exp\left[\frac{q(V+IR_s}{nKT}\right] - \frac{V}{R_{SH}} \quad \text{.....} \quad (3.3)$$

Where I is the cell output current, I_L is the light generation current, V is the voltage across the cell terminals, T is the temperature, q and k are constants, n is the ideality factor, and R_{SH} is the cell shunt resistance. While faulty solar cell design can sometimes contribute

to high levels of shunt resistance, it is more common for manufacturing flaws to be at fault when this phenomenon occurs. By offering an alternate path for the light-generated current, low shunt resistance reduces the efficiency of solar cells by reducing power output. If current is diverted away from a solar cell junction, it decreases voltage output from the cell. Light-generated current is less concentrated in low light conditions, which means that the effects of shunt resistance are magnified. To put it another way, it's much more noticeable when this current is cut off. When the solar cell's effective resistance is high, a resistance in parallel can have a substantial impact. The slope of the *I-V* curve near the short-circuit current point can be used to measure a solar cell's shunt resistance. **Fig. 3.3** depicts a schematic representation of a shunt resistance network. As can be seen in **Fig. 3.4** shunt resistance has an impact on the *I-V* curve [59].

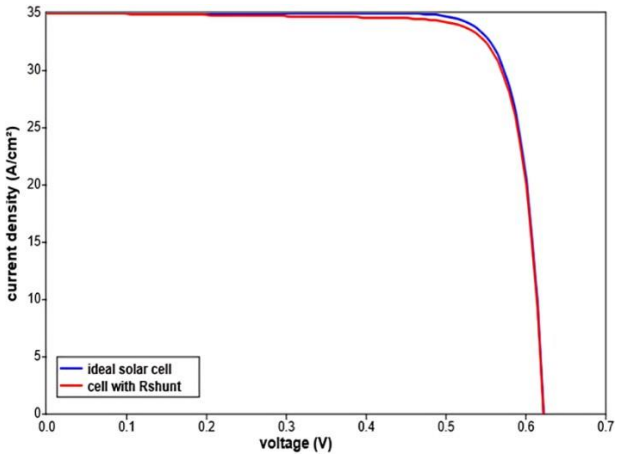

Fig. 3.4 Effect of shunt resistance on *I-V* curve

3.5 Schottky barrier height

The Schottky barrier height is one of the characteristics that makes the metal-semiconductor (MS) contact of any material so fascinating (SBH). As the SBH is the rectifying barrier for electrical conduction across the MS junction, it is of utmost significance to the proper functioning of any and all semiconductor devices. The magnitude of the SBH is a reflection of the energy disparity between the majority carrier band edge of the semiconductor and the metal Fermi level that exists across the MS interface [55]. This energy mismatch causes the SBH to exist. At the interface of a metal and an n-type semiconductor, the SBH is defined as the difference between the minimum of the conduction band and the Fermi level. And the SBH is the difference between the maximum of the valence band of the semiconductor and the Fermi level of the metal

when it comes to a p-type contact. The letter FB is the most widely used symbol for the SBH. Other superscripts and/or subscripts are sometimes added to identify the kind of semiconductor and whether the SBH refers to the flat-band condition or the depletion condition. These additions can take the form of either a superscript or a subscript. The band diagrams that demonstrate the band bending's for n-type and p-type semiconductors are typically drawn in this form and can be found rather frequently [57].

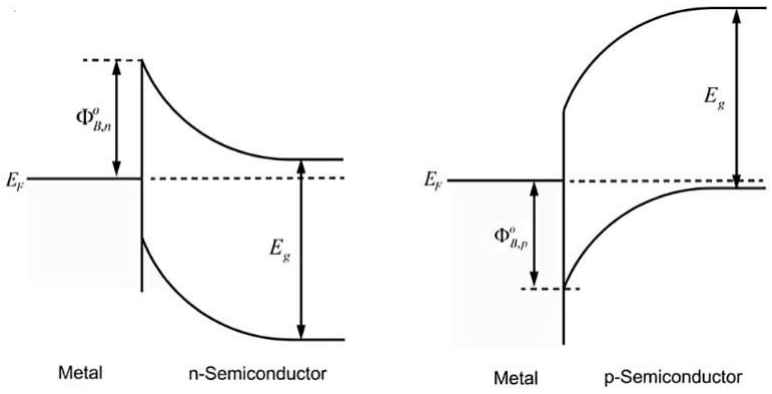

Fig. 3.5 Asymptotic band diagrams

Fig. 3.5 Illustrate how the semiconductor (or metal) bands vary as the bands approach the MS interface.

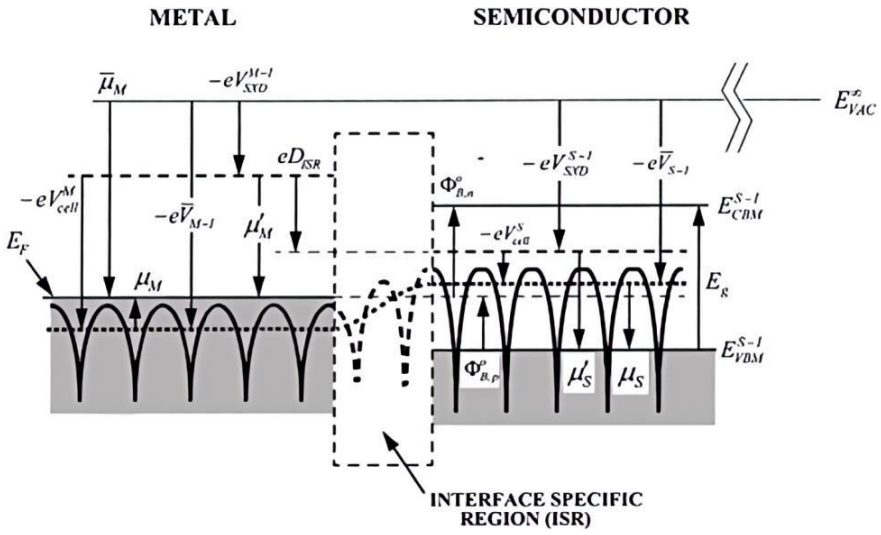

Fig. 3.6 Schottky barrier height concept

The region depicted in **Fig. 3.6** that is denoted by the little black box and given the name "interface particular region" (ISR). The magnitude of the SBH is determined here, in this transitional area between the metal and the semiconductor, which lies between the two.

3.6 Ideality factor

The diode's performance is rated by something called the ideality factor. it is dependent on V, I, temperature, and the condition of the junction. A junction between two semiconductors or a metal semiconductor junction that has a greater value of ideality factor when measured at room temperature indicates that the junction is not good enough. In order to establish the ideality factor, the slope of the linear section of the semi-log forward bias *I–V* characteristics can be calculated using the following equation:

$$n = \frac{q}{kT}\left(\frac{dv}{dInI}\right) \quad \text{.....} \quad (3.5)$$

Where $\left(\frac{dv}{dInI}\right)$ is slope of (*I-V*) curve K is the Boltzmann's constant, q is the elementary charge, T is the absolute Temperature in K.

When describing a perfect diode, the ideality factor is equal to one. In actuality, though, n is virtually always going to be greater than one [58]. The existence of a thin interfacial native oxide layer and a wide distribution of low-SBH patches can provide an explanation for the series resistance effect as well as the bias voltage dependency of SBH (or barrier inhomogeneities). When the *I–V* characteristics are examined by applying the thermionic emission theory, both the ideality factor and the barrier height decrease as the temperature drops [59]. The ideality factor, also known as n, is what is utilized in order to arrive at a conclusion regarding how near the diode adheres to pure thermionic emission. It is possible that the larger n values can be related to the widespread presence of low-SBH patches, which are caused by inhomogeneities non the lateral barrier. Image-force, recombination-generation, and tunneling could potentially be realistic mechanisms that lead to an ideality factor that is more than unity [60]. When compared to unity, the larger ideality factor value can be attributed to factors like high series resistance as well as generation and recombination currents in the depletion area. It is probable that resistive losses, leakage, shunting, or other types of bulk series resistance are the cause of the larger n values [61].

CHAPTER 4

EXPERIMENTAL STUDY

4.1 Introduction

Zinc Oxide is a semiconducting material that has been extensively researched for use in the production of DSSC, and ZnO is a competitor of TiO_2 due to characteristics such as a nearly identical band gap to TiO_2, high transparency, and ease of fabrication with various nanostructured films. ZnO with diverse nanostructures such as nanowires, nanorods, nanoflowers, or nanosheets has recently attracted attention due to its remarkable optical, electrical, and structural capabilities [62].

4.2 Experimental procedure

The whole experimental section has been done by M. S. H. Choudhury in Soga Lab, Nagoya Institute of Technology, Japan. The full experimental section can be divided as shown in **Fig. 4.1**:

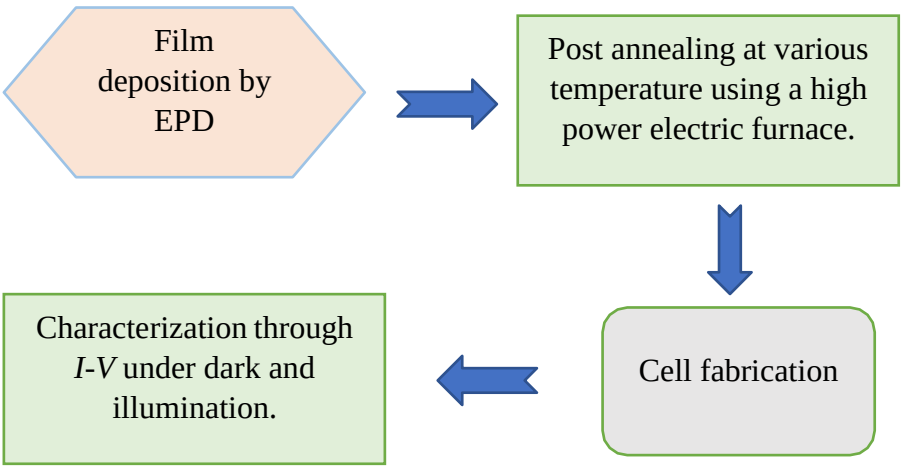

Fig. 4.1 Flow chart of experimental section

4.2.1 Film deposition by EPD

In two processes, a ZnO suspension for electrophoretic deposition was created. In ethanol, ZnO nanoparticles (100 nm, Sigma Aldrich) and acetylacetone (0.1 vol. %) were added. To break up the aggregates, acetylacetone was used. Using a homogenizer (Sonic VCX-130) at 70 percent amplitude for 10 minutes, the suspension was disseminated. Before deposition, 4% by volume of water was added to charge the solution. The mixture

was then blended with the homogenizer at 70% amplitude for 2 minutes. Prior to deposition, substrates were cleaned twice with acetone and once with methanol (5 min each time). All substrates were dried with flowing nitrogen gas and then cleaned with UV-O3. The spacing between the electrodes was 2.5 cm and 60 V DC was used during deposition. The cathode was the FTO glass substrate (2×2 cm^2) and the anode was a titanium sheet (2×2 cm^2). To create a uniform, crack-free layer of ZnO photoanodes, deposition was performed in two phases and the substrates were clipped at a 180-degree angle. After each deposition stage, the samples were dried for one minute at 80 °C. Before each deposition, the homogenizer was used for one minute to disseminate the solution. To achieve uniform deposition, the next sample was not deposited with the same solution. Total deposition time was 4 minutes.

4.2.2 Post annealing at various temperature using a high power electric furnace

The photovoltaic performance of electrophoretically formed ZnO DSCs with postannealing temperatures ranging from 100 to 550 °C was analyzed. The short circuit current density and efficiency of electrophorically deposited ZnO DSCs vary as a function of postannealing temperature. Postannealing has a significant effect on the performance of cells. The overall power conversion efficiency of the DSC without postannealing was determined to be approximately 1.53%. By raising the postannealing temperature from 100 to 450 ^oC the overall power conversion efficiency rose from 1.59 to 2.21 %.

4.2.3 Cell fabrication

During the duration of one hour, ZnO photoanodes were submerged in an ethanol solution containing 0.3 mM of a Ruthenium complex dye (Ruthenium-550 bis TBA, Solaronix). A counter electrode comprised of pt-coated glass was utilized. The electrolyte was encased in a polymer film (Himilan, 50 μm) that was connected between the two electrodes in order to both create space for it and protect it. After that, the iodide/Tri iodide redox electrolyte (Solaronix Iodolyte AN-50) was placed in that gap in between the two electrodes. Using a capillary action injector made of glass tube, the electrolyte was cautiously introduced into the system. Two standard paper clips served as the adhesive for both of the electrodes. Depending on the amount of compression pressure and temperature, the active area of the cells was approximately 0.16 cm^2, and the thickness of the film's was in the range of 12 to 17 μm (measured by alpa step 500).

4.2.4 Characterization through I-V under dark and illumination

The photovoltaic qualities were evaluated with the assistance of a solar simulator (100 $mW.cm^{-2}$, AM 1.5 illumination) in air, with the area of 0.16 cm^2 being controlled by a still mask. The photovoltaic qualities were evaluated with the use of a solar simulator, and the scanning electron microscope was used to investigate the surface morphology of the photoanodes.

CHAPTER 5

RESULTS AND DISCUSSION

5.1 Introduction

We may determine the parameter from the dark features of solar cells using three methods: the Conventional(*I-V*) Method, the Cheung Method, and the Norde Method.

5.2 Conventional I-V method

A ZnO-based dye sensitized solar cell with a dark current-voltage characteristic is depicted in **Fig. 5.1**. Voltage and Current were measured at room temperature for this experiment. The prepared DSSC's (*I-V*) characteristics are clearly nonlinear, as can be seen from the results. The series resistance, Shunt resistance, and interface state features of the device may be to blame for this divergence from linearity. In order to increase the efficiency of solar cells, this resistance must be eliminated. Series resistance and interfacial layer affect the diode's ideality factor [61]. Assuming thermionic emission is the primary process, we can derive the following relationship between Schottky diode current and voltage as [65]:

$$I = AA^{*}T^{2} \exp\left(-\frac{q\varphi_b}{K_BT}\right)\left[\exp\left(\frac{q(V-IRs)}{K_BT}\right) - 1\right] \quad (5.1)$$

Here, A is the contact area equal to 0.16cN2, φ_b is the Schottky barrier height, KB is the Boltzmann's constant, q is the elementary charge, T is the absolute temperature in K, and Rs is the series resistance. A* is the effective Richardson constant.

$$A^{*}=\frac{4\pi m^{*}k^{2}}{h^{3}} \quad (5.2)$$

where m^{*} is the effective mass of the carriers, h is the Planck constant equal to 6.634×10^{-34} J/S and A* is the Richardson constant of ZnO equal to 3.2×10^{5} $AM^{2}k^{2}$. A bias dependent Schottky Barrier Height and other effects which cause the deviation from thermionic emission are included by addition of an ideality factor (n) to eq. (5.1). The relationship between n and φ_b is given by the following expression [66]:

$$\varphi_b = \varphi_{b0} + \left(1-\frac{1}{n}\right) V \quad (5.3)$$

Here, φ_{b0} is Barrier Height under zero bias. For V-IRs>3kT/q, by using Eq. (5.1), (5.3) and (5.1) can be written as the following equation:

$$I = I_s \, exp \left[\frac{qV}{nk_BT}\right] \quad \text{(5.4)}$$

where n is the ideality factor, I_s is the saturation current, kB is the Boltzmann's constant, T is the absolute temperature and V is applied voltage. The eq. (5.4) was fitted at the lower part of the dark forward *I-V* curve in the region (V < 0.4 V). The saturation current was obtained by extrapolating the linear region of the curve to zero applied voltage. The saturation current I_s is given by [64]:

$$I_s = AA^*T^2 \, exp \left[-\frac{q\Phi_{b0}}{k_BT}\right] \quad \text{(5.5)}$$

From equation (5.4), we can write:

$$\ln (I) = In(I_s) + \frac{qV}{nKT} \quad \text{(5.6)}$$

At low and intermediate voltage region, by using eq. (5.6) the plot of ($lnI - V$) is linear and the extrapolating of this plot to *lnI* axis gives the reverse saturation current Is.

The ideality factor can be determined from the slope of ($lnI - V$) plot in according to the following equation.

$$n = \frac{q}{KT}\left(\frac{dV}{dlnI}\right) \quad \text{(5.7)}$$

Also, zero bias barrier height which is expressed by [65]:

$$\varphi_{b0} = \frac{K_BT}{q} \, ln \left(\frac{AA^*T^2}{I_s}\right) \quad \text{(5.8)}$$

Dark ($I - V$) parameters under forward and reverse bias at room temperatures for the diode can be obtained by semilogarithmic plot, Semilogarithmic plot is obtained by converting Current(I) into *Log10(I)* and **Fig. 5.1** show the semilogarithmic ($I - V$) characteristics of DSSC

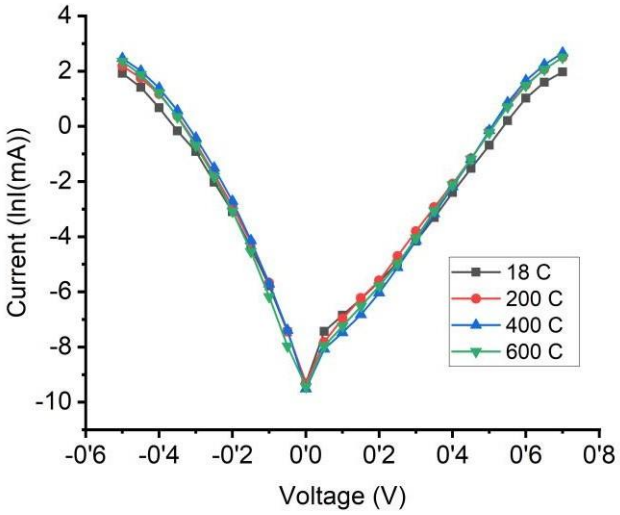

Fig. 5.1: Dark ($lnI - V$) characteristics under forward and reverse bias at room temperatures for the *ZnO* based DSSC

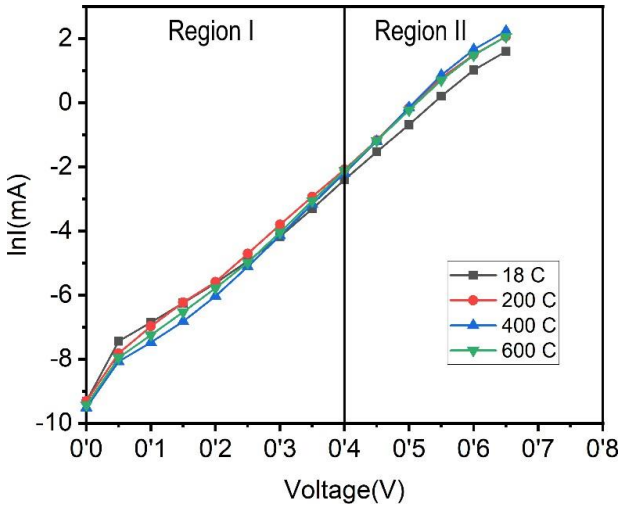

Fig. 5.2: *lnI* Versus forward voltage plot of Fig. 5.1

Using eqs. (5.6) and (5.7), The Experimental values of φ_{b0} and n for room temperature are determined from the intercept and slope of *lnI vs. V* Relation at low forward Applied voltage [68].

5.2.1 Ideality factor

We know that, ideality factor, n = $\frac{q}{KT}\left(\frac{dV}{dlnI}\right)$

Where, q = 1.6×10^{-19}JK^{-1}, K = 1.38×10^{-23} n^{2}kgs^{-2}K^{-1}, T = 298K, $\frac{dV}{dlnI} = 0.0643$

$$n = \frac{1{\cdot}6\times10^{-19}}{1{\cdot}38\times10^{-23}\times298}(0.0643)$$

$$= 2.50$$

The ideality factor for separate Dark (*I-V*) data is obtained by taking individual slope of ($lnI - V$) curve, that are included in data Table.

5.2.2 Saturation current (I_0)

Saturation current is needed for calculation of zero bias barrier height which were discuss above and given in the table.

5.2.3 Zero bias barrier height

We Know that, Zero bias Barrier Height,

$$\varphi_{b0} = \frac{K_B T}{q} ln\left(\frac{AA^* T^2}{I_s}\right)$$

Where, $K_B = 1.38 \times 10^{-23}\ M^2kgs^{-2}K^{-1}$, T = 298K, $q = 1.6 \times 10^{-19}JK^{-1}$, A =0.16$Cm^2$,

$A^* = 3.2 \times 10^9 A/cm^2k^2$, $I_s = 1.67*10^{-4}$

$$\varphi_{b0} = \frac{1.38\times10^{-19}\times298}{1{\cdot}6\times10^{-19}} ln\left(\frac{0.16\times3.2\times10^{-19}\times298^2}{1.67\times10^{-4}}\right) = 1.032$$

The Zero Bias barrier height for separate Dark (*I-V*) data is obtained by taking individual Intercept of ($lnI - V$) curve, that are included in **Table 5.1**

5.2.4 Series and Shunt resistance

In order to determine the effect of series resistance and shunt resistance on the solar cell during dark condition, we used the conventional method. By using *I–V* curves, we can determine the junction resistance, where $Rj = \frac{\partial v}{\partial i}$, Rj represent both series resistance and shut resistance. **Fig. 5.4** show the plot of junction resistance (Rj) against the applied voltage(V) [70].

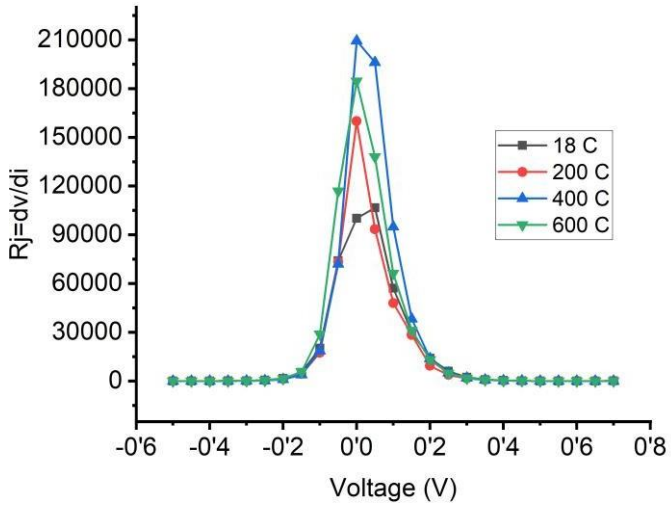

Fig. 5.3: Rj versus Applied Voltage(V) plot

From the **Fig. 5.3** we consider High value of shunt resistance and low value of series resistance. In the case of reverse bias potential, we can determine shunt resistance from Rj versus Voltage(V) plot. Similarly, we can also determine series resistance from Rj versus Voltage(V) plot, for forward bias potential. Series resistance and shunt resistance determined from **Fig. 5.3** Rs =22.12 (ohm), Rsh = 74067.49 (ohm) respectively.

Table 5.1 We obtained saturation currents, ideality factor and the zero-bias barrier height values, Series and shunt Resistance values from Fig. 5.2 and Fig. 5.3 by using conventional *I-V* method.

Tem *(°C)*	**FF**	**η (%)**	**Pmax (mW)**	**Saturation current *(I_o)***	**Ideality factor *(n)***	**Barrier height *(φ_{b0})*** (eV)	**Shunt resistance, Rsh (Ω)**	**Series resistance, Rs (Ω)**
18	0.530	2.11	1.454	1.67×10^{-4}	2.50	1.032	74067.49	22.12
200	0.525	2.31	2.311	1.34×10^{-4}	2.27	1.037	73339.59	11.55
400	0.528	2.42	2.429	1.01×10^{-4}	2.22	1.045	72068.95	10.05
600	0.579	2.40	2.407	1.27×10^{-4}	2.25	1.039	116857.92	11.55

From **Table 5.1** the analytically obtained data of ZnO based DSSCs, it is explicit that when the Schottky barrier is higher than 0.5eV, a momentous reduction in the FF and

power generated per unit area of the cell. The extracted barrier is found to increase with temperature and this are explained on the basis of the bias dependence of the potential barrier at the ZnO interface [69]. We find the barrier height are 1.032 to 1.039 eV for ZnO based Dye sensitize solar cell. So, we can assume a reduction of FF is 5% and the above 96% reduction in the P_{max} are deduced. The Calculated high barrier height of ZnO based Dye sensitize solar cell which indicate the large value of series resistance. In the case of the ideality factor, greater than unity exhibits the presence of non-ideal behavior in (*I-V*) characteristics at lower voltages. From table-5.1 we can see that when the annealing temperature is between 18 and 400 ^{o}C, the ideality factor decreases with increasing barrier height. And when the annealing temperature is above 400 ^{o}C, the ideality factor increases as the barrier height decreases. Therefore, if the ideality factor increases, the barrier height decreases. The Saturation Current increases as temperature increases. The higher value of n may be due to potential drop in the interfacial layer and presence of excess current and the recombination current through the interfacial states between the metal/insulator layers [69]. Also, Series and shunt resistance decreases when the temperature is between 18 and 400 ^{o}C, but the value of both resistance increases when it is 400 degrees higher or 600 ^{o}C.

5.3 Cheung- Cheung functions

Cheung developed another method for calculating Schottky diode series resistance from a single *I-V* measurement, in addition to barrier height and ideality factor. The Cheung approach is built on a modified TE model, Cheung's equations [67]:

$$\frac{dV}{dlnI} = IRs + \frac{nKT}{q} \quad \ldots\ldots\ldots\ldots\ldots\ldots\ldots\ldots\ldots\ldots\ldots\ldots\ldots\ldots\ldots\ldots \quad (5.9)$$

$$H(I)=V - \frac{nKT}{q} In(\frac{1}{AA^{*}T^{2}}) \quad \ldots\ldots\ldots\ldots\ldots\ldots\ldots\ldots\ldots\ldots\ldots\ldots\ldots\ldots\ldots\ldots \quad (5.10)$$

$$H(I)=IR_s + n\varphi_b \quad \ldots\ldots\ldots\ldots\ldots\ldots\ldots\ldots\ldots\ldots\ldots\ldots\ldots\ldots\ldots\ldots \quad (5.11)$$

Plotting d(V)/d(InI) against I(A) will provide a straight line in the region of the (*I-V*) characteristic with an intercept and slope that give the values of n and Rs, respectively, in accordance with eq. (5.9).

We Know that, $\frac{dV}{dlnI} = IRs + \frac{nKT}{q}$

5.3.1 Series resistance

Where Rs = 15.93 Ω. Similarly, some value of series resistance was taken from the d(V)/d(*lnI*) against I(A) which are include in the table below.

5.3.2 Ideality factor

$\frac{nKT}{q} = 0.05381$

Where, k $= 1.38 \times 10^{-23} m^2 \text{kgs}^{-2}\text{K}^{-1}$, T $= 298\text{K}$, q $= 1.6 \times 10^{-19}\text{JK}^{-1}$

now n= $\frac{0.05381 \times 1{\cdot}6 \times 10^{-19}}{1{\cdot}38 \times 10^{-23} \times 298}$

= 2.09

Substituting the value of n and the data of the same voltage range in Eq. (5.10) produce *H(I)* Then a plot of *H(I)* versus *I(A)* according to eq. (5.11) should result also in a straight line with a slope of IRS and intercepts at y-axis. Another value of nφ_b. Rs can be obtained from eq. (5.11). Two values of the diode resistance can be used as a measure of these methods' accuracy [65]. In this work, we already determined the value of Zero bias barrier height for ZnO based Dye sensitize solar cell under dark condition by using Convention method, as temperature is same, zero bias barrier height are skipped for C*h*eung-C*h*eung function and eq. (5.11) are also skipped. In the **Table 5.2**, the value of n and Rs determined for (*lnI-V*) data of **Fig. 5.2** by considering forward bias potential.

Table 5.2. Ideality factor and Series Resistance values obtained by using Cheung's method for **Fig 5.2**

Temp *(°C)*	**FF**	**η (%)**	**Pmax (mW)**	**Ideality factor (n)**	**Series resistance, Rs (Ω)**
18	0.530	2.11	1.454	2.09	15.93
200	0.525	2.31	2.311	1.96	17.02
400	0.528	2.42	2.429	1.95	17.99
600	0.579	2.40	2.407	1.94	17.37

In **Table 5.2** As the temperature rises the ideality factor decreases and the series resistance increases. Annealing temperature at 18 to 400 ℃ increasing of Rs value,

decreases the fill factor (FF) and increasing efficiency & maximum power but after 400 °C efficiency (η) and maximum power were decreased with Series Resistance (Rs) decreased and fill factor increased.

5.4 Norde Method

The Norde method is an alternate way for determining series resistance. It is defined by the function listed below [71]:

$$F(V)=\frac{v}{2}-\frac{KT}{q}\ln\left(\frac{I}{AA^{*}T^{2}}\right) \quad \text{.....} \quad (5.12)$$

Here in eq. (5.12) is the applied voltage, I is the current in the device, A is the contact area of the diode, A * is the effective Richardson constant, T is the absolute temperature, q is the electronic charge, and k is the Boltzmann constant.

Now, the barrier height and series resistance are

$$\varphi_b = F(V_{min}) + \frac{v_{min}}{2} - \frac{KT}{q} \quad \text{.....} \quad (5.13)$$

$$R_s=\frac{kT}{qI_0} \quad \text{.....} \quad (5.14)$$

And Bohlin suggested the generalized Norde function to determine φ_b and Rs values from a single *I-V* measurement at a constant temperature. The generalized Norde function is characterized as follows [71]:

$$F(v,\alpha)=\frac{v}{\alpha}-\frac{KT}{q}\ln\left(\frac{I}{AA^{*}T^{2}}\right) \quad \text{.....} \quad (5.15)$$

α is defined as an arbitrary constant greater than n, β is equal to q/kT, I(V) is extracted from the measured *I-V* curve. φ_b and Rs values can be obtained by determining of F(V,α) against V plot minimum in according to following equations:

$$\varphi_b = F_{min}(v,\alpha) + \left(\frac{\alpha-n}{n}\right)\left(\frac{v_0}{\alpha}-\frac{KT}{q}\right) \quad \text{.....} \quad (5.16)$$

$$R_s=\frac{(\alpha-n)}{\beta I_{min}} \quad \text{.....} \quad (5.17)$$

where n value is obtained from the *lnI-V* plot. Fmin (V, α) is the minimum point F(V, α)-V plot, Vmin and Imin are the corresponding voltage and current, respectively.

5.4.1 Barrier height

The barrier height is measured by the difference in potential between the metal's Fermi energy and the edge of the band where the majority of carriers live. Symbolically, it is referred to as φ_b.

5.4.2 Series resistance

Transparent conductive oxide (TCO), electrolyte layer, and counter electrode create series resistances in DSSC, which have an effect on the device's performance. The primary effect of series resistance is a decrease in the fill factor; however, extremely high values may also have the effect of lessening the short-circuit current.

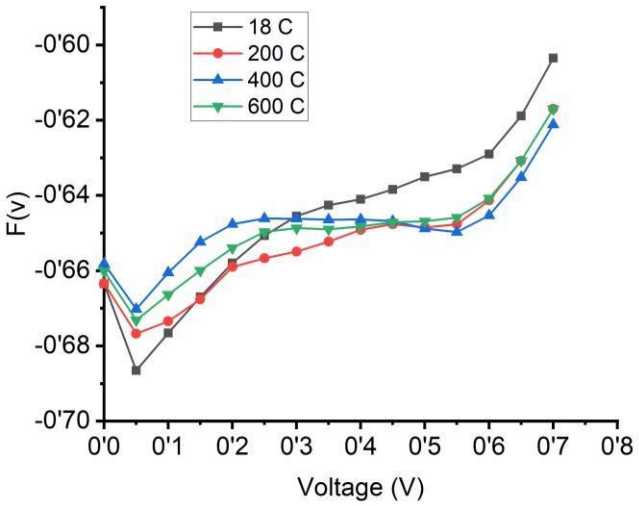

(a)

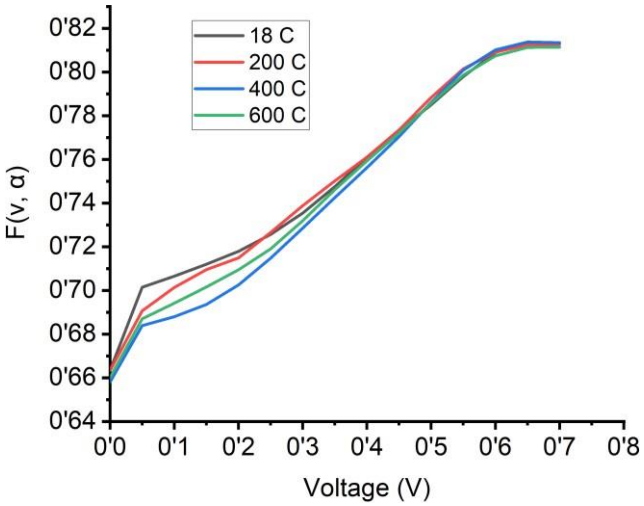

(b)

Fig. 5.4: ***(a)*** F(V) versus Applied Voltage(V) plot for Norde method

(b) F(V) versus Applied Voltage(V) plot for Norde Generalized Method

Table 5.3. Barrier height and Series Resistance values obtained by using Norde and Norde Generalized Method for Fig. 5.4

Temp ***(°C)***	**FF**	**η (%)**	***Jsc*** **(mA/cm^2)**	**Norde Method**		**Norde Generalized Method**	
				Barrier height (φ_b)	**Series Resistance (Rs)**	**Barrier height (φ_b)**	**Series Resistance (Rs)**
18	0.530	2.11	6.69	1.47 eV	3.75 Ω	1.17 eV	9.38 Ω
200	0.525	2.31	8.06	1.48 eV	2.88 Ω	1.20 eV	6.53 Ω
400	0.528	2.42	8.43	1.49 eV	2.18 Ω	1.22 eV	4.84 Ω
600	0.579	2.40	7.61	1.48 eV	2.43 Ω	1.21 eV	5.48 Ω

As shown in **Table 5.3**, from varying annealing temperature of the DSSC cell from 18 ^{o}C to 600 ^{o}C. We observed open-circuit voltage (Voc) and short-circuit current density (Jsc), where (Jsc) increases from 6.691250 (mA/cm^2) at 18 ^{o}C to reach maximum value of 8.433125 (mA/cm^2) at 400 ^{o}C with an increase in the power conversion efficiency (η) from 2.114062 to 2.429437 (%). But at 600 ^{o}C temperature short-circuit current density (Jsc) were decreased at 7.617500 (mA/cm^2) within decreased efficiency (η) at 2.407000 (%).

The effect of annealing temperature variation was clearly observed in series (Rs) resistance **Table 5.3**. The value of series resistance was 3.75 Ω for annealed 18 ^{o}C, with gradual increase in annealing temperature to 400 ^{o}C the value of Rs decreased to 2.18 Ω. But at annealed 600 ^{o}C the value of Rs increased at 2.43 Ω.

We also show the reduction of FF against the increment efficiency (η) of for solar cells with various Series resistance and overall, the increase in T depicted a decrease in FF. The FF value is related to Voc, Rs and Rsh. Both the Rs and the Rsh values of the solar cells affect the FF value.

5.5 Illuminated Current-Voltage characteristics

The determination of the dc current-voltage characteristic of photovoltaic cells under the influence of varying intensities of white light illumination is one of the standard procedures used in the characterization of photovoltaic cells. A sample was exposed to a high-power tungsten lamp from an appropriate distance in order to evaluate the photo response of the constructed ZnO-based DSSCs [63]. This was done at an acceptable distance in order to prevent the thermal heating of the cell. The photocurrent–photovoltage characteristics of ZnO-based DSSCs are depicted in **Fig. 5.5**. These features are shown to be affected by varying levels of illumination. This graphic illustrates the region of the (*I-V*) readings that falls within the fourth quadrant at a variety of various light levels. The photocurrent and photovoltage clearly rose as the applied illumination increased. According to analysis, dye sensitization of semiconductor materials results in high photovoltages but low photocurrents. This was determined through evaluation. The self-quenching and aggregation of particles are mostly to blame for this phenomenon [72].

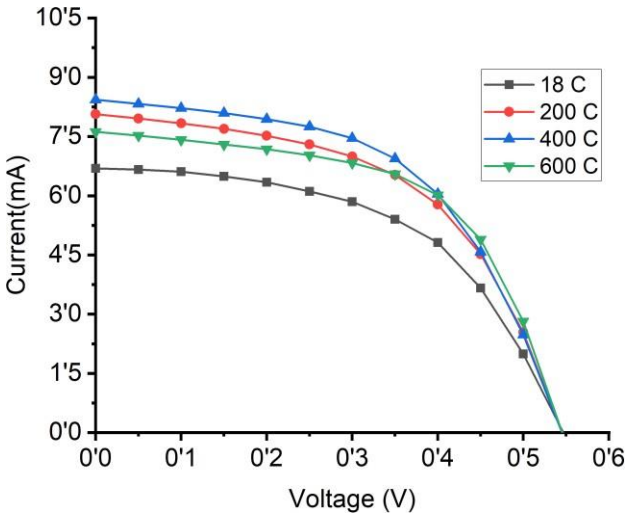

Fig. 5.5 Current versus Voltage plot under illumination

5.5.1 Resistance

The resistance of the solar cell is one of the primary parameters that may have a significant impact on the total power conversion efficiency of DSSC. There are two forms of resistance that may have an impact on efficiency. The *I-V* characteristic of DSSC may be used to determine the resistance, as illustrated in the picture.

5.5.2 Series resistance

The series resistance of DSSC is caused by TCO sheet resistance, incorrect ionic diffusion in the electrolyte, contact resistance, and counter electrode/electrolyte interface resistance. The resistance in series would be zero in an ideal situation. On the (*I-V*) curve, the slope close to the point Voc may be used to get an estimate of the series resistance.

5.5.3 Shunt resistance

Leakage current into the cell as a result of impurities or faults introduced during the manufacturing process is the root cause of shunt resistance. Ideally, resistance should be pushed into infinity such that there is no further current route. A smaller open circuit voltage is a byproduct of the reduced shunt resistance. Shunt resistance may be determined by the inverse of slope near the point, short circuit current Isc on the *I-V* curve.

Table 5.4: Series and shunt Resistance values of *I-V* Characteristics under illumination

Temp *(°C)*	**FF**	**η (%)**	**Pmax (mW)**	**Shunt Resistance, Rsh (Ω)**	**Series resistance, Rs (Ω)**
18	0.530	2.11	1.454	501.85	15.61
200	0.525	2.31	2.311	195.91	10.16
400	0.528	2.42	2.429	271.37	13.72
600	0.579	2.40	2.407	229.37	8.85

Table 5.4 shows that the series and shunt resistance decrease when the annealing temperature is 18 to 200 ℃ but increases again at 400 ℃. And decreasing again after 400 ℃ . And we also show that efficiency and maximum power increased at temperature 18 to 400 ℃ but after 400 ℃ both were decreased.

5.6 Comparison between conventional and Cheung method

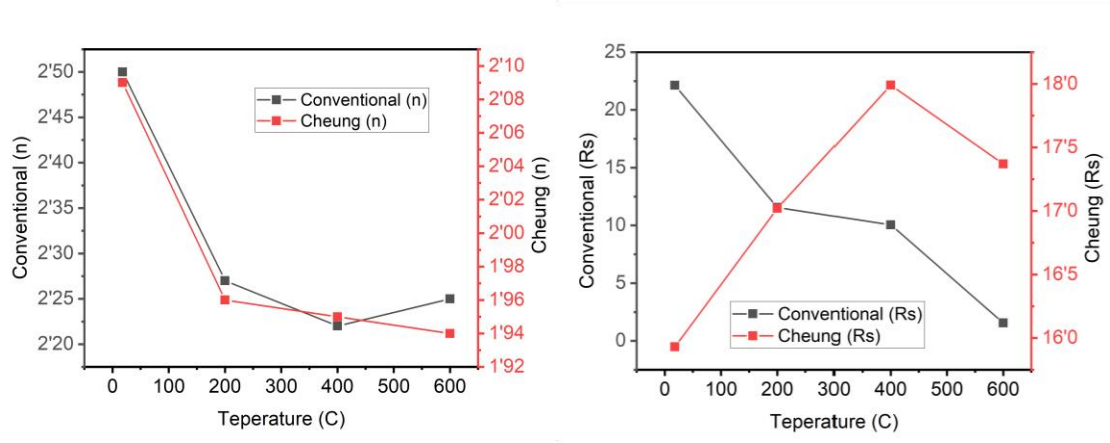

(a) **(b)**

Fig. 5.6: (a) Temperature vs Ideality factor of Cheung and Conventional method

(b) Temperature vs Series Resistance of Cheung and Conventional method

The *I–V* characteristics of the DSSC are nonlinear. This variation may be caused by the device's series resistance, shunt resistance, and interface state. This resistance has an impact on the performance of solar cells and must thus be monitored. Conventional methods were used to figure out how series and shunt resistance affect the properties of a ZnO desensitized solar cell. Using this method, the shunt resistance rises as the reverse bias potential increases. Similarly, when there is a significant forward bias potential, it results in a small, practically constant resistance. In contrast, the series resistance created by the Cheung technique is substantially lower than the usual way. Take into consideration each individual data set's particular inclination and it may have led to its occurrence. In terms of how close they get to the perfect solution; from **Fig. 5.6** we can see that the two approaches are almost identical. The height of the barrier changes as the temperature changes, but these (*I-V*) measurements were gathered at room temperature, which explains why the results varied so little.

5.7 Comparison between conventional and Norde method

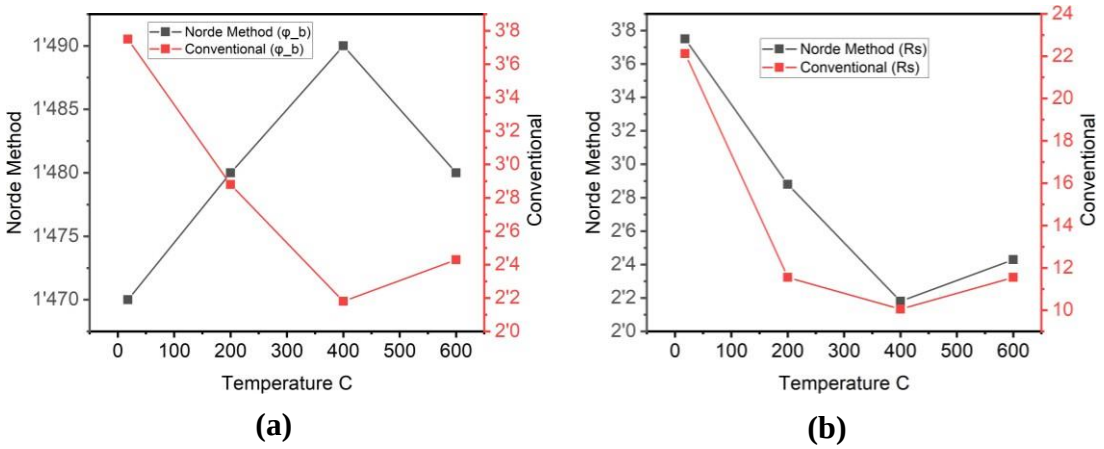

Fig. 5.7: (a) Temperature vs Barrier height of Norde and Conventional method

(b) Temperature vs Series Resistance of Norde and Conventional method

At room temperature, we evaluated the electrical properties of DSCC by measuring its current and voltage (*I-V*) using a variety of techniques, and the results are presented in the table below as barrier heights and series resistance. In order to determine diode parameters like the ideality factor (n), series resistance (Rs), and barrier height (φ_b), Cheung and Norde's approach was used to conduct *I-V* measurements. Comparing the ideality factor and barrier height values computed with Cheung functions using various approaches, it was determined that they were in accord. However, the parameters acquired from Cheung functions and Norde's functions do not accord with one another. Cheung functions, on the other hand, are solely applied to the nonlinear area (high voltage zone) of the forward bias *I–V* characteristics. In contrast, the complete forward bias *I–V* characteristics of the junctions are taken into account when using Norde's functions.

The heights of the barriers calculated with the traditional *I-V* method are pretty close to those calculated with the more general Norde method. Form **Fig. 5.7** we can see that the conventional *I-V* approach and the Norde method do not match up consistently with one another.

5.8 Comparison between Resistance of *(I-V)* data under dark condition and Resistance of *(I-V)* under illumination

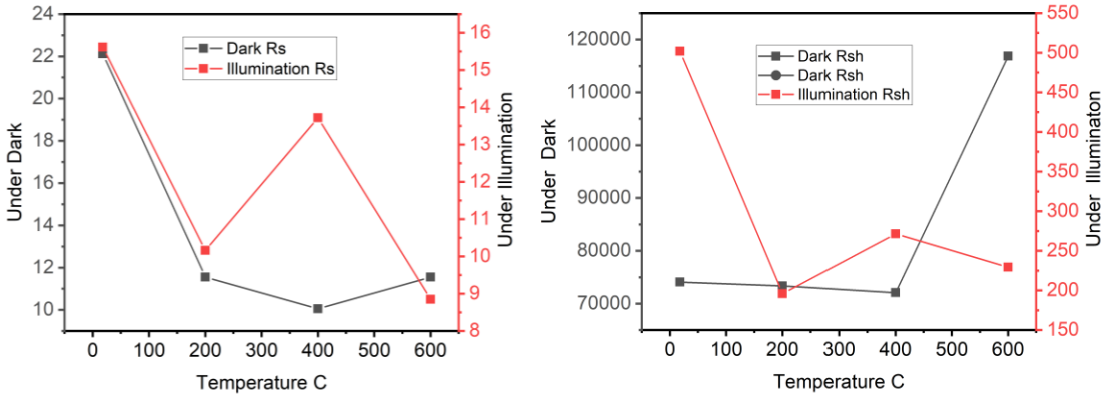

(a) **(b)**

Fig. 5.8:(a) Temperature vs Series Resistance Under Dark condition and Illumination

(b) Temperature vs Shunt Resistance Under Dark condition and Illumination

From the **Fig. 5.8** we see that series resistance are almost same both dark and illumination condition but between shunt resistance has huge difference under both conditions. The shunt resistance was about 501.85 ohm under lighting, whereas the series resistance was around 15.61 ohm; a high shunt resistance indicates that the device performed well under illumination. Furthermore addition, DSSCs have a high shunt resistance of dark (*I-V*), which allows them to absorb more light in overcast situations than silicon-based photovoltaic cells. This advantage gives DSSCs a competitive advantage over silicon-based photovoltaic cells.

CHAPTER 6

CONCLUSION AND FUTURE WORK

6.1 Conclusion

In this study, we analyze ZnO based Dye sensitize solar cell and its Current-Voltage characteristics at room temperature under dark condition. At low biasing voltages, the electrical conduction processes of the constructed ZnO-based DSSC were investigated. The thermionic emission at lower voltage managed the device's mechanism. The measured non-ideal I-V curve was used to determine the series resistance values, ideality factors, and barrier heights. Series resistance and ideality factor has been calculated from forward bias potential by using Cheung function have small difference with conventional method. Also, device series resistance and shunt resistance has been checked by analyzing current-voltage characteristics under illumination. Series resistance and barrier heights were fined from Norde function. The influence of annealing temperature was also examined for each of the compositions, and it was determined that 400 ℃ was the optimal temperature for achieving the highest possible level of productivity. The most effective charge separation was achieved as a result of the presence of TiO_2, which was responsible for the significant improvement in photovoltaic performance. Although it was discovered that the metals boosted the efficiency, it was discovered that increasing the content led to a fall in the efficiency. Therefore, the ideal concentrations of Ag and Pd might potentially operate as electron traps, which would speed up the process of electron-hole separation. Therefore, photoanodes loaded with noble metals as well as valonia as a source of carbon are a possible alternative to photoanodes loaded with zinc oxide. In addition to that, the findings of this study offer fresh perspectives on the composite photoanodes that are utilized in DSSCs.

6.2 Future work

Because of its direct wide band gap (3.3 eV), large exciton binding energy (60 meV), high infrared reflectivity, high electrochemical stability, excellent electronic properties, and cost effectiveness compared to TiO_2 as photoanode, ZnO is being used more frequently in the fabrication of DSSCs in the current decade [74]. In the future, there are also plans to conduct a study using natural dyes rather than Eosin Y ($C_{20}H_6Br_4Na_2O_5$) in order to gain a better understanding of the efficiency of photoelectron production in ZnO-based DSSCs.

REFERENCES

[1] O'regan, B. and Grätzel, M., "A low-cost, high-efficiency solar cell based on dye-sensitized colloidal TiO2 films", *nature*, *353*(6346), pp.737-740, 1991.

[2] Akhtar, M.S., Khan, M.A., Jeon, M.S. and Yang, O.B., "Controlled synthesis of various ZnO nanostructured materials by capping agents-assisted hydrothermal method for dye-sensitized solar cells", *Electrochimica Acta*, *53*(27), pp.7869-7874, 2008.

[3] Joshi, L.P., Poudel, Y., Nakarmi, M.L., Niraula, P.R. and Shrestha, S.P., "Preparation and Characterization of Zinc Oxide Based Photoanode for Dye-sensitized Solar Cell using Delonix Regia Natural Dye Extract", *Journal of Nepal Physical Society*, *4*(1), pp.1-6, 2017.

[4] Dye-sensitized solar cell. (2022, July 16). https://en.wikipedia.org/w/index.php?title=Dye-sensitized_solar_cell&oldid=1098489530

[5] Teesetsopon, P., Kumar, S. and Dutta, J., "Photoelectrode optimization of zinc oxide nanoparticle based dye-sensitized solar cell by thermal treatment", *Int. J. Electrochem. Sci*, *7*(6), pp.4988-4999, 2012.

[6] Singh, S., Singh, A. and Kaur, N., "Imine-linked receptors decorated ZnO-based dye-sensitized solar cells", *Bulletin of Materials Science*, *39*(6), pp.1371-1379, 2016.

[7] Pauporté, T., "Optimizing Light Harvesting and Charge Collection in Dye-Sensitized Solar Cells Based On ZnO", *ECS Transactions*, *58*(11), p.29, 2013.

[8] Pandey, P., Parra, M.R., Haque, F.Z. and Kurchania, R., "Effects of annealing temperature optimization on the efficiency of ZnO nanoparticles photoanode based dye sensitized solar cells", *Journal of Materials Science: Materials in Electronics*, *28*(2), pp.1537-1545, 2017.

[9] Kutlu, N., "Investigation of electrical values of low-efficiency dye-sensitized solar cells (DSSCs)", *Energy*, *199*, p.117222, 2020.

[10] Syukron, A., Wahyuono, R.A., Sawitri, D. and Risanti, D.D., "The effect of paste preparation and annealing temperature of zno photoelectrode to dye-sensitized solar cells (dssc) performance", *Advanced Materials Research* (Vol. 896, pp. 183-186), 2014.

[11] Khan, J. and Arsalan, M.H., "Solar power technologies for sustainable electricity generation–A review. *Renewable and Sustainable Energy Reviews*, *55*, pp.414-425, 2016.

[12] Gong, J., Sumathy, K., Qiao, Q. and Zhou, Z., "Review on dye-sensitized solar cells (DSSCs): Advanced techniques and research trends", *Renewable and Sustainable Energy Reviews*, *68*, pp.234-246, 2017.

[13] Kazmi, S.A., Hameed, S., Ahmed, A.S., Arshad, M. and Azam, A., "Electrical and optical properties of graphene-TiO2 nanocomposite and its applications in dye sensitized solar cells (DSSC)", *Journal of Alloys and Compounds*, *691*, pp.659-665, 2017.

[14] Hegazy, A., Kinadjian, N., Sadeghimakki, B., Sivoththaman, S., Allam, N.K. and Prouzet, E., "TiO2 nanoparticles optimized for photoanodes tested in large area Dye-sensitized solar cells (DSSC)", *Solar Energy Materials and Solar Cells*, *153*, pp.108-116, 2016.

[15] Snaith, H.J., "Estimating the maximum attainable efficiency in dye-sensitized solar cells", *Advanced Functional Materials*, *20*(1), pp.13-19, 2010.

[16] Sengupta, D., Das, P., Mondal, B. and Mukherjee, K., "Effects of doping, morphology and film-thickness of photo-anode materials for dye sensitized solar cell application–A review", *Renewable and Sustainable Energy Reviews*, *60*, pp.356-376, 2016.

[17] Wu, J., Lan, Z., Lin, J., Huang, M., Huang, Y., Fan, L., Luo, G., Lin, Y., Xie, Y. and Wei, Y., "Counter electrodes in dye-sensitized solar cells', *Chemical Society Reviews*, 46(19), pp.5975-6023, 2017.

[18] Fujishima, A. and Honda, K., "Electrochemical photolysis of water at a semiconductor electrode", *nature*, *238*(5358), pp.37-38, 1972.

[19] Gaikwad, M. A., Suryawanshi, M. P., Desai, S. P. and Moholkar, A. V., "ZnO-based photoelectrodes for dye sensitized solar cell via modified successive ionic layer adsorption and reaction route", *International Journal of Engineering Research and Technology*, vol. 10, No. 1, pp. 55-560, 2017.

[20] Zinc oxide. (2022, June 23). https://en.wikipedia.org/w/index.php?title=Zinc_oxide&oldid=1094667526

[21] Umar, A. and Hahn, Y.B. eds., 2010. "Metal Oxide Nanostructures and Their Applications," *American Scientific Publishers, Stevenson Ranch*, 2010.

[22] Physical properties (2022, June 23). https://en.wikipedia.org/wiki/Zinc_oxide#Physical_properties

[23] Haynes, J.R., "Experimental proof of the existence of a new electronic complex in silicon",*Physical Review Letters*, *4*(7), p.361, 1960.

[24] Uthirakumar, A., *Fabrication of ZnO Based Dye Sensitized Solar Cells*, in L. A. Kosyachenko (ed.), Solar Cells - Dye-Sensitized Devices, London, 2011, pp. 436-451.

[25] Ferrere, S., Zaban, A. and Gregg, B.A., 'Dye sensitization of nanocrystalline tin oxide by perylene derivatives", *The Journal of Physical Chemistry B*, *101*(23), pp.4490-4493, 1997.

[26] Bergeron, B.V., Marton, A., Oskam, G. and Meyer, G.J., "Dye-sensitized SnO2 electrodes with iodide and pseudohalide redox mediators", *The Journal of Physical Chemistry B*, *109*(2), pp.937, 2005.

[27] Nusbaumer, H., Moser, J.E., Zakeeruddin, S.M., Nazeeruddin, M.K. and Grätzel, M., "CoII (dbbip) 22+ complex rivals tri-iodide/iodide redox mediator in dye-sensitized photovoltaic cells", *The Journal of Physical Chemistry B*, *105*(43), pp.10461-10464, 2001.

[28] Wu, J., Lan, Z., Hao, S., Li, P., Lin, J., Huang, M., Fang, L. and Huang, Y., "Progress on the electrolytes for dye-sensitized solar cells", *Pure and Applied Chemistry*, *80*(11), pp.2241-2258, 2008.

[29] Toivola, M., Ahlskog, F. and Lund, P., "Industrial sheet metals for nanocrystalline dye-sensitized solar cell structures", *Solar energy materials and solar cells*, *90*(17), pp.2881-2893, 2006.

[30] Deepa, H.A., Madhu, G.M. and Venkatesham, V., "Performance evaluation of DSSC's fabricated employing TiO2 and TiO2-ZnO nanocomposite as the photoanodes", *Materials Today: Proceedings*, *46*, pp.4579-4586, 2021.

[31] Baxter, J.B., Walker, A.M., Van Ommering, K. and Aydil, E.S., "Synthesis and characterization of ZnO nanowires and their integration into dye-sensitized solar cells", *Nanotechnology*, 17, S304. S304, 2006.

[32] Park, K., Zhang, Q., Garcia, B.B., Zhou, X., Jeong, Y.H. and Cao, G., "Effect of an ultrathin TiO2 layer coated on submicrometer-sized ZnO nanocrystallite aggregates by atomic layer deposition on the performance of dye-sensitized solar cells", *Advanced Materials*, *22*(21), pp.2329-2332, 2010.

[33] Grätzel, M., "Dye-sensitized solar cells", *Journal of photochemistry and photobiology C: Photochemistry Reviews*, *4*(2), pp.145-153, 2003.

[34] Zhang, Q., Dandeneau, C.S., Zhou, X. and Cao, G., "ZnO nanostructures for dye-sensitized solar cells", *Advanced materials*, *21*(41), pp.4087-4108, 2009.

[35] Wu, J.J., Chen, G.R., Lu, C.C., Wu, W.T. and Chen, J.S., "Performance and electron transport properties of TiO2 nanocomposite dye-sensitized solar cells", *Nanotechnology*, *19*(10), p.105702, 2008.

[36] Li, Z., Yu-Qing, F., Mao-Cong, Z., Min, W., Jia-Yu, Z., Chun-Xiang, X. and Yi-Ping, C., "Performances of ZnO-based dye sensitized solar cells fabricated by hydrothermal synthesis and sol-gel technique", *Chinese Physics Letters*, *26*(1), p.018401, 2009.

[37] Yu, H., Zhang, S., Zhao, H., Will, G. and Liu, P., "An efficient and low-cost TiO2 compact layer for performance improvement of dye-sensitized solar cells", *Electrochimica Acta*, *54*(4), pp.1319-1324, 2009.

[38] Gnida, P., Jarka, P., Chulkin, P., Drygała, A., Libera, M., Tański, T. and Schab-Balcerzak, E., "Impact of TiO2 nanostructures on dye-sensitized solar cells performance", *Materials*, *14*(7), p.1633, 2021.

[39] Bagher, A.M., Vahid, M.M.A. and Mohsen, M., "Types of solar cells and application", *American Journal of optics and Photonics*, *3*(5), pp.94-113, 2015.

[40] Ranabhat, K., Patrikeev, L., Antal'evna-Revina, A., Andrianov, K., Lapshinsky, V. and Sofronova, E., "An introduction to solar cell technology", *Journal of Applied Engineering Science*, *14*(4), pp.481-491, 2016.

[41] Solar Cell, (2020, October 28). https://www.electrical4u.com/solar-cell/

[42] Kibria, M.T., Ahammed, A., Sony, S.M., Hossain, F. and Islam, S.U., "A Review: Comparative studies on different generation solar cells technology", *Proc. of 5th International Conference on Environmental Aspects of Bangladesh* (pp. 51-53), 2014.

[43] Sharma, S., Jain, K.K. and Sharma, A., "Solar cells: in research and applications—a review", *Materials Sciences and Applications*, *6*(12), p.1145, 2015.

[44] Hussein, A.M., Iefanova, A.V., Koodali, R.T., Logue, B.A. and Shende, R.V., "Interconnected ZrO2 doped ZnO/TiO2 network photoanode for dye-sensitized solar cells", *Energy Reports*, *4*, pp.56-64, 2018.

[45] Anta, J.A., Guillén, E. and Tena-Zaera, R., "ZnO-based dye-sensitized solar cells",*The Journal of Physical Chemistry C*, *116*(21), pp.11413-11425, 2012.

[46] Wang, P., Zakeeruddin, S.M., Moser, J.E., Nazeeruddin, M.K., Sekiguchi, T. and Grätzel, M., "A stable quasi-solid-state dye-sensitized solar cell with an amphiphilic ruthenium sensitizer and polymer gel electrolyte", *Nature materials*, *2*(6), pp.402-407, 2003.

[47] Bai, Y., Cao, Y., Zhang, J., Wang, M., Li, R., Wang, P., Zakeeruddin, S.M. and Grätzel, M., "High-performance dye-sensitized solar cells based on solvent-free electrolytes produced from eutectic melts", *Nature materials*, *7*(8), pp.626-630, 2008.

[48] Chiba, Y., Islam, A., Watanabe, Y., Komiya, R., Koide, N. and Han, L., "Dye-sensitized solar cells with conversion efficiency of 11.1%", *Japanese journal of applied physics*, *45*(7L), p.L638, 2006.

[49] González-Verjan, V.A., Trujillo-Navarrete, B., Félix-Navarro, R.M., de León, J.N., Romo-Herrera, J.M., Calva-Yáñez, J.C., Hernández-Lizalde, J.M. and Reynoso-Soto, E.A., "Effect of TiO2 particle and pore size on DSSC efficiency", *Materials for Renewable and Sustainable Energy*, *9*(2), pp.1-8, 2020.

[50] Omar, A., Ali, M.S. and Abd Rahim, N., "Electron transport properties analysis of titanium dioxide dye-sensitized solar cells (TiO2-DSSCs) based natural dyes using electrochemical impedance spectroscopy concept: A review", *Solar Energy*, *207*, pp.1088-1121, 2020.

[51] Sharma, K., Sharma, V. and Sharma, S.S., "Dye-sensitized solar cells: fundamentals and current status", *Nanoscale research letters*, *13*(1), pp.1-46, 2018.

[52] Saturation Current, (2020, September 23). https://en.wikipedia.org/w/index.php?title=Saturation_current&oldid=979982373

[53] Dark Current, (2022, July 16). https://en.wikipedia.org/w/index.php?title=Dark_current_(physics)&oldid=1098566044

[54] Currents through the diode (in the dark), (2022, July 10). https://www2.pvlighthouse.com.au/resources/courses/altermatt/The%20PV%20Principle/Currents%20through%20the%20diode%20%28in%20the%20dark%29.aspx

[55] Series Resistance, (2022, July 10)., https://www.pveducation.org/pvcdrom/solar-cell-operation/seriesresistance.

[56] Shunt Resistance, (2022, July 10)., https://www.pveducation.org/pvcdrom/solar-cell-operation/shuntresistance

[57] Çaldıran, Z., Deniz, A.R., Aydoğan, Ş., Yesildag, A. and Ekinci, D., "The barrier height enhancement of the Au/n-Si/Al Schottky barrier diode by electrochemically formed an organic Anthracene layer on n-Si", *Superlattices and Microstructures*, *56*, pp.45-54, 2013.

[58] El-Menyawy, E.M. and Ashery, A., "Current–voltage characteristics and inhomogeneous barrier height analysis of Au/poly (o-toluidine)/p-Si/Al heterojunction diode", *Journal of Materials Science: Materials in Electronics*, *25*(9), pp.3939-3946, 2014.

[59] Güllü, Ö., Asubay, S., Aydoğan, Ş. and Türüt, A.B.D.U.L.M.E.C.İ.T., "Electrical characterization of the Al/new fuchsin/n-Si organic-modified device", *Physica E: Low-dimensional Systems and Nanostructures*, *42*(5), pp.1411-1416, 2010.

[60] Tozlu, C. and Mutlu, A., "Poly (melamine-co-formaldehyde) methylated effect on the interface states of metal/polymer/p-Si Schottky barrier diode", *Synthetic Metals*, *211*, pp.99-106, 2016.

[61] Joshi, L.P., Poudel, Y., Nakarmi, M.L., Niraula, P.R. and Shrestha, S.P., "Preparation and Characterization of Zinc Oxide Based Photoanode for Dye-sensitized Solar Cell using Delonix Regia Natural Dye Extract", *Journal of Nepal Physical Society*, *4*(1), pp.1-6, 2017.

[62] Wahyuono, R.A. and Risanti, D.D., "Modeling and experiment of dye-sensitized solar cell with vertically aligned ZnO nanorods through chemical bath deposition", *International Seminar on Photonics, Optics, and Its Applications (ISPhOA 2014)* (Vol. 9444, pp. 142-147)., 2015.

[63] Hafez, H.S., Yahia, I.S., Sakr, G.B., Abdel-Mottaleb, M.S.A. and Yakuphanoglu, F., "Extraction of the DSSC parameters based TiO2 under dark and illumination conditions", *Adv. Mater. Corros*, *1*, pp.8-13, 2012.

[64] Aldemir, D.A., Kökce, A. and Özdemir, A.F., "The comparison of the methods used for determining of Schottky diode parameters in a wide temperature range", *Sakarya Üniversitesi Fen Bilimleri Enstitüsü Dergisi*, *21*(6), pp.1286-1292, 2017.

[65] Wahyuono, R.A. and Risanti, D.D., "January. Modeling and experiment of dye-sensitized solar cell with vertically aligned ZnO nanorods through chemical bath deposition", *International Seminar on Photonics, Optics, and Its Applications (ISPhOA 2014)* (Vol. 9444, pp. 142-147)., 2015.

[66] Rani, M. and Tripathi, S.K., "A comparative study of nanostructured TiO2, ZnO and bilayer TiO2/ZnO dye-sensitized solar cells", *Journal of Electronic Materials*, *44*(4), pp.1151-1159, 2015.

[67] Abuelwafa, A.A., El-Denglawey, A., Dongol, M., El-Nahass, M.M., Ebied, M.S. and Soga, T., "On the electrical characterization of platinum octaethylporphyrin (PtOEP)/Si hybrid device", *Applied Physics A*, *124*(1), pp.1-12, 2018.

[68] Pillai, P.B., Corpus Mendoza, A.N., De Souza, M.M., Bree, G. and Jeng, D., "Extraction of Schottky barrier at the F-doped SnO2/TiO2 interface in Dye Sensitized solar cells", *Journal of Renewable and Sustainable Energy*, *6*(1), p.013142, 2014.

[69] Darwish, S., Riad, A.S. and Soliman, H.S., "Electrical conductivity and the effect of temperature on photoconduction of n-ZnSe/p-Si rectifying heterojunction cells", *Semiconductor science and technology*, *11*(1), p.96, 1996.

[70] Shah, M., Sayyad, M.H., Karimov, K.S. and Maroof-Tahir, M., "Investigation of the electrical properties of a surface-type Al/NiPc/Ag Schottky diode using I–V and C–V characteristics", *Physica B: Condensed Matter*, *405*(4), pp.1188-1192, 2010.

[71] Bohlin, K.E., "Generalized Norde plot including determination of the ideality factor", *Journal of Applied Physics*, *60*(3), pp.1223-1224, 1986.

[72] Güler, G., Güllü, Ö., Karataş, Ş. and Bakkaloğlu, Ö.F., "March. Analysis of the series resistance and interface state densities in metal semiconductor structures", In *Journal of Physics: Conference Series* (Vol. 153, No. 1, p. 012054). 2009.

[73] Zhang, S., Yang, X., Numata, Y. and Han, L., "Highly efficient dye-sensitized solar cells: progress and future challenges", *Energy & Environmental Science*, *6*(5), pp.1443-1464, 2013.

[74] Thomas, S., Deepak, T.G., Anjusree, G.S., Arun, T.A., Nair, S.V. and Nair, A.S., “A review on counter electrode materials in dye-sensitized solar cells”, *Journal of Materials Chemistry A*, *2*(13), pp.4474-4490, 2014.